DECENTRALIZED PRODUCTION OF FISCHER-TROPSCH BIOCRUDE VIA CO-PROCESSING OF WOODY BIOMASS AND WET ORGANIC WASTE IN ENTRAINED FLOW GASIFICATION: TECHNO-ECONOMIC ANALYSIS

Gonzalo Del Alamo[a], Rajesh S. Kempegowda[a], Øyvind Skreiberg[a], Roger Khalil[a]

[a]SINTEF Energy Research, Kolbjorn Hejes vei 1A, 7491, Trondheim, Norway

KEYWORDS: biocrude, co-processing, wood, organic waste, entrained flow gasification, Fischer Tropsch, techno-economics

ABSTRACT. The present work addresses the techno-economics of the decentralized co-production of Fischer-Tropsch biocrude and Liquefied Natural Gas via thermo-chemical conversion of woody biomass and wet organic waste to syngas in an entrained flow gasification

reactor. The process design considers thermal pretreatment of the feedstock based on integrated drying of both the woody biomass and the organic waste using direct-contact superheated steam, and torrefaction for the dried wood. The super-heated steam required for drying is produced from recovery of residual heat from the main conversion process. The overall cost of biocrude production has been shown to decrease when increasing the fraction of organic waste when considering gate fees for the organic waste, at the production site, above 10 $/ton. For gate fees of 50 $/ton, which are realistic for the current waste market, the cost of biocrude ranges between 25 and 22 $/GJ for plant scales between 150 and 600 MW based on the input feedstock energy to the entrained flow gasification. Although the sludge has lower calorific value and higher moisture content, which require higher capital investment for pretreatment, the reduction of feedstock supply cost with increasing fraction of sludge becomes dominant in evaluating the overall cost of production. Moreover, the overall efficiency for biocrude and LNG production, and therefore the main income to the plant, is comparable for mass fractions of the sludge in the raw feedstock ranging between 0 and 50%. Based on direct-contact superheated steam dryers for the pretreatment of sludge, the residual heat recovered from the main conversion process is sufficient to co-process up to 50% mass fraction of sludge in the raw feedstock with moisture content up to 80%.

1. INTRODUCTION

The combustion of fossil fuels for transportation is a main contributor to the total greenhouse gas emissions related to human activities, accounting for about 23% worldwide [1], 23% in Europe [2], 26% in the US [3] and 33% in Norway [4]. In this context, the use of biofuels in the transport sector has been proposed as part of wider global strategies for moving into low-carbon

societies through replacement of fossil fuels [5]. The role of biofuels has been particularly emphasized for the heavy-duty transport sectors, i.e. aviation, maritime and long-haul trucks, which do not have in the near future viable alternatives to reduce fossil carbon emissions other than using liquid biofuels.

Among several technological options [6, 7] for producing liquid biofuels that meet or exceed current market specifications, Entrained flow gasification (EFG) of biomass followed by the catalytic Fischer-Tropsch synthesis (FTS) exhibits several technological advantages that makes it attractive for achieving full commercial deployment: 1) the high-energy density as well as the high cold gas efficiency in the entrained flow gasification [8,9] and 2) the high quality of the product from the Fischer-Tropsch synthesis, which is compatible with conventional refinery processes for upgrading to marketable biodiesel-type fuels (with lower sulphur content and better cetane number than fossil-based diesel) and aviation fuels [10]. However, the progress in commercialization of this technology route has been limited mainly due to the large scales required in order to achieve the economic viability [10,11]. Large plant capacities impact significantly in the economics of liquid biofuels production due to the financial risks associated with large capital investments and on the complex logistics and high cost of feedstock supply. The effect of feedstock supply may be even more critical for countries like Norway where the costs of biomass transport is especially significant.

In this context, decentralized production of biocrude with further upgrading in conventional refineries is a relevant strategy for improving the overall economics of liquid biofuels production since it reduces the capital investment by utilizing existing petrochemical infrastructure and thus reduces the viable plant capacity. The authors have already addressed the techno-economics of decentralized production of biocrude based on conversion of dried and torrefied woodchips via

EFG and FTS with utilization of excess heat for coproduction of hot water and electricity [12]. This work showed that, under Norwegian conditions, the cost of production of Fischer Tropsch biocrudes and co-producing only heat for district heating can be in the range of 30 to 24 $/GJ for plant capacities between 150 and 600 MW. It also showed that co-production of electricity in Norway increases the cost of biocrude production up to 40% due to the high capital cost of the power production system and the low electricity prices. However, although co-production of heat theoretically improves the economics of biocrude production, there is a practical limitation in the amount of heat that can be exported to district heating networks, since biocrude production plants would be located close to the forest. On the other hand, when considering the conversion of biomass to biocrude with plant capacities in the range of 150 to 600 MW, the costs of feedstock supply become significant and can represent about 26-38 % of the total operating cost of the plant [12].

The present work evaluates the decentralized production of Fischer-Tropsch biocrudes by co-processing woody biomass and dewatered sludge in an entrained flow gasifier. This represents a new strategy, not addressed in the literature before, that can potentially improve the economics of biocrude production by reducing the cost of feedstock supply and through a better utilization of the residual heat recovered from the overall conversion process. The co-processing strategy also adds a higher-degree of flexibility in the plant operation based on variations of the feedstock availability and prices. Sludge residues from anaerobic digestion are an abundant, continuously available and renewable feedstock. Based on official statistical data, the availability of sludge from urban waste water plants, food processing industry and biogas production in Norway is approximately 4.8 millions tons per year, respectively, which represent approximately 5.8 TWh.

Depending on the composition, sludge residues are spread on soils for agricultural purposes with zero cost at production site or diverted to incineration also subjet to gate fees.

The methodology used in the present work involves a parametric analysis of the biocrude production plant, with derivation of explicit expressions to evaluate the overall techno-economic performance under variable plant scales. The parameters considered in the analysis include process design and operation, dimensioning and costing of the main equipment. Both the process and economics are described in terms of the scale of the plant and the operational limits of the gasification system. The scale of the plant has been described as the input feedstock energy flow to the gasification system. This analysis included in this work reports explicit parametric expressions to evaluate the overall process and economic performance of the proposed technological route, which are not currently available in the literature.

2. PROCESS DESIGN AND MODELLING

Figure 1 shows the overall process block diagram of the biocrude production plant based on co-processing wood and organic waste, including the main mass and energy flows, with $\dot{M}$, $\dot{H}$ and $\dot{Q}$ denoting mass flow rate, total enthalpy flow and heat flow, respectively. The main process steps include thermal pretreatments of the woody biomass and the organic waste, for reducing the moisture content and the particles size of the feedstock, high-temperature oxygen-enriched entrained flow gasification (EFG) followed by syngas cooling and conditioning and Fischer-Tropsch synthesis (FTS) with separation of hydrocarbon products. The main product of the plant is the so-called biocrude, which is here defined as the mixture of hydrocarbons produced from the FTS with carbon number above 3. The plant includes co-production of liquefied natural gas (LNG) from the gas stream after separation, which is composed of hydrocarbon with carbon number 1-3. Further refining of the bio-crude to marketable liquid biofuels, based on

conventional refinery processes, has been excluded from the analysis in this work. Available heat from the syngas cooling and the FTS is here recovered for production of superheated steam, which is utilized for pretreatment of the feedstock as well as for the gasification and WGS processes. The net excess heat from the plant is exported for district heating. The main parameter considered to describe the scale of the plant is the input feedstock power to the EFG, denoted by $\dot{H}_S^G$. A more detailed description of the main systems, including main process design and operational parameters, is presented in the following sections.

2.1. FEEDSTOCK PROPERTIES

This work considers three types of feedstock: logwood containing stem wood and bark, woodchips derived from forest residues, mainly tops and branches, and dehydrated sludge from anaerobic digestion. All woody biomass is based on spruce, which is the most common species in the Norwegian forest industry. Each input feedstock to the plant is characterized by the mass flow rate $\dot{M}_J^F$, the Net Calorific Value per dry basis NCV_J^F, the volatiles, moisture, ash and fix carbon content (proximate analysis), $y_{J,v}^F$, $y_{J,H2O}^F$, $y_{J,a}^F$ and $y_{J,fc}^F$ respectively, the elemental composition (ultimate analysis) $y_{J,i}^F$, and the particle size $d_{p,J}^F$. The moisture content is here considered a variable parameter depending on the specific characteristics of each feedstock supply chain. Table 1 shows the characteristics, including proximate and ultimate analysis and heating values, of the feedstock considered in this work under representative Norwegian conditions. It has been assumed that the logwood consists on 90% stem wood and 10% bark. The moisture content of the green logwood varies in the range of 40-60% depending on the wood species, forest location and season of harvesting. The particle size of woodchips is in the range of is 30 to 50 mm. Dehydrated sludge is assumed to have a moisture content in the range of 60-80 % wt.

2.2. FEEDSTOCK PRETREATMENT

The process flow diagram of the complete feedstock pretreatment system is shown in Figure 2. Pretreatment of the logwood include chipping and screening, drying, torrefaction and milling. Bark, which has a higher ash content compared to stem wood, is not separated before chipping in order to increase the overall ash content in the input biomass to the entrained flow gasification. Fines, containing particles with size below 1 mm, are collected and introduced directly into the gasifier. Torrefaction of the woody biomass improves the grindability and energy density of the input feedstock to gasification leading to a better economic performance of the overall biocrude production compared to pretreatment based on conventional drying only, as it has been proven already in a previous work by the authors [12]. Pretreatment of the sludge includes drying and grinding. Steam produced from the heat recovery system of the plant is utilized as the heating medium for drying both the woodchips and the sludge. The heat produced from combustion of the volatiles released from torrefaction is used both for heating the feedstock in the torrefaction reactor and the steam after the sludge dryer and prior the woodchips dryer.

Logwood chipping and screening

Chipping and screening is described based on the output particle size distribution, shown in Table 2, according to data from Laitila et al. [14], and the total power consumption W^{CS} calculated from

$$W^{CS} = w^{CS}\dot{M}_s^{CS} \ , \tag{2.1}$$

where $\dot{M}_s^{CS}$ is the input mass flow rate of raw logwood and $w^{CS}$is the specific energy consumption per unit input mass, assumed to be constant and equal to 6.9 kWh/ton based on experimental results with disc chippers by Spinelli et al. [15]. Screening is performed for particle

size in the range of 1 and 45 mm. Particles above 45 mm are recycled back to the chipper, while fines below 1 mm are fed directly in the EFG.

Dryers

Direct-contact steam dryers has been considered for pretreatment of both the woody biomass and the sludge. The overall process performance of the drier is described in terms of the required input thermal power of the drying agent $\dot{Q}_g^D$, which is calculated from

$$\dot{Q}_g^D = \dot{M}_s^D \left[q_s^D + \Delta y_{H_2O}^D h_{g,o}^D\right]/\left(1 - h_{g,o}^D/h_{g,i}^D\right), \quad (2.2)$$

where $\dot{M}_s^D$ is the mass flow rate of feedstock entering the dryer, $q_s^D = \Delta y_{H_2O}^D h_{H2O}^v + c_{p,s}^D \Delta T_s^D$ is the heat transfer per unit mass of feedstock, $\Delta y_{H_2O}^D = \left(y_{H_2O}^F - y_{H_2O}^D\right)$ and ΔT_s^D=$(T_s^F - T_s^D)$ are the variation in the moisture content and the temperature in the feedstock, $h_{g,i}^D$ and $h_{g,o}^D$ are the specific enthalpies of the drying agent at the inlet and outlet, h_{H2O}^v is the vaporization enthalpy of water and $c_{p,s}^D$ is the average specific heat capacity of the feedstock. It has been assumed that the outlet temperature of the feedstock is equal to the saturation temperature of water at the dryer pressure and the outlet temperature of the drying agent is 20 °C above the saturation point.

Dimensioning of the drier has been described in terms of the volume V_r^D and external surface area A_r^D, which are evaluated using a lumped capacity approximation for the solid particles based on a heat transfer area between the drying agent and the solid particles, which is evaluated from $A_{gs}^D = V_r^D(1 - \phi_s^D)/d_p$, giving

$$V_r^D = \dot{M}_s^F\left[\Delta y_{H_2O}^D h_{H2O}^v + c_{p,s}^D \Delta T_s^D\right]/\left[4U_{gs} LMTD_{gs}^D\,(1 - \phi_s^D)/d_p\right] \quad (2.3)$$

and

$$A_r^D = 2q_s^D/\left[LMTD_{gs}^D U_{gs}\,(1 - \phi_s^D)^{3/2}/d_p\right]\left\{\dot{M}_s^F/[v_s^D \rho_s^D (1 - \phi_s^D)\pi]\right\}^{1/2} \quad (2.4)$$

where ρ_s^D, ϕ_s^D and v_s^D are, respectively, the average density, specific heat capacity, bed porosity and velocity of the biomass in the dryer, $LMTD_{gs}^D = \left[\left(T_{g,i}^D - T_s^F\right) - \left(T_{g,o}^D - T_s^D\right)\right] Ln\left[\left(T_{g,i}^D - T_s^F\right)/\left(T_{g,o}^D - T_s^D\right)\right]$ is the log mean temperature difference and $U_{gs} = (k_g/d_p)[1 + (4/\phi_s^D)(1 - \phi_s^D)]\left[(1 - \phi_s^D)^{1/2} Pr^{1/3} Re_{d_p}^{0.6}\right]$ is the overall gas to solid heat transfer coefficient U_{gs} obtained by Kuwahara et al. [16] for packed beds with porosities in the range of 0.2 to 0.9, where $Re_{d_p} = 4\rho_s^D v_s^D (1 - \phi_s^D)\left(\dot{M}_g^D/\dot{M}_s^D\right) d_p/\left(\mu_g \phi_s^D\right)$ is the characteristic Reynolds number based on the particle size and the average velocity of the solid in the dryer v_s^D, which is assumed to be constant and equal to 0.02 m/s.

Torrefaction

The torrefaction process for each type of feedstock is described in terms of experimental results obtained by Tapasvi et al. [13] of the proximate and ultimate composition, the heating value and the density of the solid product as a function of the temperature T_s^T and the residence time t_r^T of the solid particles inside the torrefaction reactor. The design of the torrefaction reactor is based on a vertical tower with a height to diameter ratio equal to 2, where the volume of the torrefaction reactor is calculated from

$$V_r^T = t_r^T \dot{M}_j^F \left(1 - \Delta y_{j,H_2O}^D\right)/[\rho_s^T (1 - \phi_s^T)], \quad (2.5)$$

where $\Delta y_{j,H_2O}^D$ is the variation in moisture content of the feedstock in the drying process prior torrefaction, ρ_s^T and ϕ_s^T are the average feedstock density and gas to solid volume ratio in the torrefaction reactor. In this work, it is assumed that ϕ_s^T is constant and equal to 0.82.

Particle size reduction

Particle size reduction is performed by grinding in hammer mills. The characterization of the particle size reduction is based on the output particle size distribution $f^{SR}(d_p)$ and the total electric power consumed $\dot{W}_e^{SR}$which is calculated from

$$\dot{W}_e^{SR} = \dot{M}_S^{SR} w_e^{SR} \tag{2.6}$$

where $\dot{M}_S^{SR}$ is the input feedstock mass flow rate and w_e^{SR} is the specific electric energy consumed per unit input mass, dependent on the particle size and the process condition in the torrefaction process. In this work, we have assumed a linear decrease of the grinding energy with increasing values of the torrefaction temperature in the range of 200 to 300 °C given by the empirical formula $w_e^{SR} = 125 - (T_s^T - 200)$ based on experimental data Govin et al. [17].

Mass and energy yields for the overall pretreatment system

Considering the integrated pretreatment of woody biomass and organic waste shown in Figure 2, explicit expressions for the total mass and energy yields, denoted by f_s^{PR} and ϵ_s^{PR}, can be obtained in terms of the input and output composition and calorific value of the feedstock and the conditions of the drying agent, giving

$$f_s^{PR} = \sum\left(Y_j^F f_j^{PR}\right) \tag{2.7}$$

and

$$\epsilon_s^{PR} = \sum\left(Y_j^F LHV_j^F \epsilon_j^{PR}\right) / \sum\left(Y_j^F LHV_j^F\right), \tag{2.8}$$

Where $f_j^{PR} = 1 - \Delta y_{j,H_2O}^{PR} - \left(1 - y_{j,H_2O}^F\right)\Delta y_{j,v}^{PR}$ and $\epsilon_j^{PR} = 1 + \left[\Delta y_{j,H_2O}^{PR} h_{H2O}^v + c_{j,s}\Delta T_s^{PR} - \left(1 - y_{j,H_2O}^F\right)\left[LHV_{j,dry}^F - \left(1 - \Delta y_{j,v}^{PR}\right)LHV_{j,dry}^{PR}\right]\right] / LHV_j^F$ are the mass and energy yields from the pretreatment of each feedstock, with $\Delta y_{j,H_2O}^{PR}$, $\Delta y_{j,v}^{PR}$ and

ΔT_S^{PR} denoting respectively the variation of the feedstock moisture, volatiles and temperature during pretreatment.

2.3. GASIFICATION, COOLING AND CONDITIONING

Figure 3 shows the process flow diagram for the gasification and the syngas cooling and conditioning systems. Thermochemical conversion of the biomass to syngas is performed in an entrained flow gasifier operated with oxygen-enriched air and steam. The syngas from the EFG reactor is cooled with recovery of heat for production of superheated steam. The process design for the syngas cooling includes a radiative and convective water-tube evaporation of saturated water, super-heating of saturated steam, gas-tube boiler and economizer for preheating the temperature of the feed water. After cooling, removal of particulate matter is performed with bag filters. Increase of the H_2 to CO molar ratio of the syngas to the value required by FT synthesis is performed by complete water-gas shifting of a fraction f_{wgs} of the total syngas flow. Heat recovery after the WGS reactor is performed in a boiler with production of saturated steam. The temperature of the syngas in the boiler is kept above the saturation temperature to avoid water condensation. Removal of CO_2 and H_2S from the shifted syngas is performed in a Selexol system. This technology is suitable for the range of CO_2 removal efficiencies required, which varies within 82-90% depending on the initial syngas composition, and exhibits low H_2 and CO losses [18]. Selexol also allows pure pressure-swing process configurations and minimize the energy consumption for thermal regeneration in the range of CO_2 removal efficiencies considered. The Selexol system includes syngas cooling with free condensed water removal in a water knock-out drum, the absorber where the syngas is in direct contact with the lean Selexol solvent, and the solvent regeneration unit. Regeneration of the Selexol is performed in three flash drums, operating at 10, 6.5 and 1.1 bar. The flash gas from the first two flash drums contains

considerable amounts of H_2 and CO, and is therefore recycled to the absorber to minimize the losses of these components. The flashed gas from the near-atmospheric regeneration stage is a high-purity CO_2 stream which is further compressed and cooled for storage in liquid phase. After regeneration, the lean Selexol is cooled by fresh water before entering the absorber.

EFG reactor

The EFG process has been assumed to be adiabatic and is described in terms of the input feedstock energy flow, composition and calorific value, denoted by $\dot{H}_S^G$, $y_{S,i}^G$ and LHV_S^G, the lambda value or air-fuel equivalence ratio λ_g, here defined as the ratio of the actual molar flow rate of oxygen used for gasification to the total stoichiometric molar flow rate needed for complete combustion, the total steam to carbon molar ratio $(S/C)_g$, the oxygen concentration in the gasification air X_{O2}^{ASU} and the reactor pressure P_g^G. The calorific value and composition of the input feedstock are evaluated from

$$LHV_S^G = \sum\left(\epsilon_j^{PR} Y_j^F \left(1 - y_{j,H2O}^F\right) LHV_{j,dry}^F\right) / \sum\left(Y_j^F \left(1 - y_{j,H2O}^{PR}\right) f_j^{PR}\right), \quad (2.9)$$

$$y_{S,i}^G = \sum\left[Y_j^F f_j^{PR} \left(1 - y_{j,H2O}^{PR}\right) y_{j,i}^{PR}\right] / \sum\left[Y_j^F f_j^{PR} \left(1 - y_{j,H2O}^{PR}\right)\right] \quad (2.10)$$

and

$$y_{S,H2O}^G = \sum\left(Y_j^F y_{j,H2O}^{PR}\right) / \sum\left(Y_j^F f_j^{PR}\right), \quad (2.11)$$

where ϵ_j^{PR} and f_j^{PR} are the mass and energy yields from the pretreatment of each feedstock, $y_{S,i}^G$ denotes the dry composition with the subscript i representing volatiles, fixed carbon, ash and atomic composition and the superscripts F and PR denoting conditions of raw feedstock and after pretreatment, respectively. The total input mass flow rate of feedstock and the molar flow rate of gasification air and steam to the EFG can then be obtained from $\dot{M}_S^G = \dot{H}_S^G / LHV_S^G$, $\dot{N}_{air}^G = \left(\dot{H}_S^G / LHV_S^G\right) n_{air}^G$ and $\dot{N}_{stm}^G = \left(\dot{H}_S^F / LHV_S^G\right) n_{stm}^G$, where

$$n_{air}^G = \left(\lambda_g / X_{O2}^{ASU}\right)\left(1 - y_{S,a}^G - y_{S,H_2O}^G\right)(1 + x/4 - y/2)/(W_C + yW_O + xW_H), \quad (2.12)$$

and

$$n_{stm}^{G} = \left[(S/C)_g \left(1 - y_{S,a}^{G} - y_{S,H_2O}^{G}\right)/(W_C + yW_O + xW_H) - y_{S,H_2O}^{G}/W_{H2O}\right]. \quad (2.13)$$

are the moles of gasification air and steam per unit mass of input feedstock. The outlet syngas flow from the EFG is described in terms of the molar flow rate $\dot{N}_g^G = \dot{M}_s^G n_g^G$, temperature T_g^G and composition, $x_{g,i}^G$, where n_g^G are the moles of syngas per unit input mass of feedstock to the EFG calculated from

$$n_g^G = \frac{\left(1-y_{S,a}^{G}-y_{S,H_2O}^{G}\right)}{W_g^G}\left[1 + \left(\frac{\lambda_g}{X_{O2}^{ASU}}\right)\frac{X_{O2}^{ASU}W_{O2}+(1-X_{O2}^{ASU})W_{N2}}{W_C+yW_O+xW_H} + \frac{W_{H_2O}(S/C)_g}{W_C+yW_O+xW_H}\right]. \quad (2.14)$$

In equations (2.12-2.14), W_g^G is the mean molecular weight of syngas and $x = \left(W_C y_{S,H}^G\right)/\left(W_H y_{S,C}^G\right)$ and $y = \left(W_C y_{S,O}^G\right)/\left(W_O y_{S,C}^G\right)$ are, respectively, the H/C and O/C atomic ratios of the input feedstock, with W_i denoting the atomic weight. Calculation of the outlet temperature and the syngas composition has been done by simulating the gasification process in Aspen using thermochemical equilibrium based on Gibbs free energy minimization applied to the elemental gas composition (C, H, O, N, and S) of the input solid, subject to char gasification and water-gas reactions [19]

$$C_{(s)} + H_2O \rightarrow CO + H_2 \quad (R1)$$

$$C_{(s)} + CO_2 \rightarrow 2CO \quad (R2)$$

$$C_{(s)} + 0.5O_2 \rightarrow CO \quad (R3)$$

$$C_{(s)} + 2H_2 \rightarrow CH_4 \quad (R4)$$

$$S + H_2 \rightarrow H_2S \quad (R5)$$

$$CO + H_2O \leftrightarrow CO_2 + H_2 \quad (R6)$$

together with the energy conservation equation

$$n_g^G\left[\bar{c}_{p,g}^G\left(T_g^G - T^0\right) + \sum\left(x_{g,,i}^G\,\overline{LHV_i}\right)\right] + n_{air}^G\bar{c}_{p,air}^G\left(T_{air}^G - T^0\right) + n_{stm}^G W_{H_2O} h_{stm}^G + y_{S,a}^G\left[c_a^G(T_a^G - T^0) + y_{a,C}^G LHV_C\right] - LHV_S^G = 0, \quad (2.15)$$

where $\bar{c}_{p,i}^G$, c_a^G, T_i^G denotes the specific heat and temperature of the syngas, gasification air and ash, $T^0 = 298\,K$ is a reference temperature, $y_{a,C}^G$ and $LHV_C = 34.1\,MJ/kg$ are the carbon content in the ash and the calorific value per unit mass of carbon, $\overline{LHV_i}$ are the calorific value per unit mole of each component of the syngas and $h_{stm}^G$is the specific enthalpy of the steam. Slag is quenched and transported to a silo by chain and band conveyors. It is assumed that 95% of the ash content in the feedstock is in the slag, the remaining 5% being transferred as particulate matter to the output syngas flow.

Air separation and compression

The air separation unit (ASU) shown in Figure 3 represent a complete package including fresh air heating and compression, cryogenic cooling and separation, specified in terms of the total flow rate of O_2 that needs to be separated, $\dot{N}_{O_2}^{ASU} = \left(\dot{H}_s^G/LHV_S^G\right)n_{air}^G(X_{O2}^{air} - X_{O2}^{ASU})$, with n_{air}^G given by equation (2.12). Assuming that the outlet pressure from the ASU unit is atmospheric, the compressor for the oxygen-enriched air to the EFG reactor is specified based on the total electric power required for compression to the EFG pressure, calculated from

$$w_{air}^G = \left(\dot{H}_s^G/LHV_S^G\right)n_{air}^G(R/W_{O2})(T_{air}^G/T^0)P_{atm}\left[\left(P_g^G/P_{atm}\right)^{\frac{n-1}{n}} - 1\right]n/(n-1) \quad (2.16)$$

where T_{air}^G is the outlet air temperature from the separation unit and n is the polytropic coefficient of the compressor.

Gas cooling train

The overall syngas cooling train is described in terms of the pressure and temperature conditions of the superheated steam produced, denoted by P_{stm}^{GC} and T_{stm}^{GC}, and the outlet temperature of the

syngas $T_{g,i}^{WGS}$, here specified as the minimum inlet temperature to the water-gas shifting required for activation of the catalysts. The total steam power produced from the syngas cooling can then be calculated from

$$\dot{Q}_{stm}^{SC} = \left(\dot{H}_s^G / LHV_S^G\right) n_g^G \left(h_g^G - h_g^{WGS}\right) / \eta_{th}^{SC}, \quad (2.17)$$

where h_g^G and h_g^{WGS} are the thermal enthalpy of syngas at the EFG outlet conditions and at the WGS inlet conditions, respectively, and η_{th}^{SC} is the thermal efficiency of the overall cooling train. Dimensioning of each section J of the gas cooling train is based on the total heat transfer area A_{th}^J, calculated from $A_{ht}^J = \dot{M}_g^G c_{p,g}^J \left(T_{g,o}^J - T_{g,i}^J\right) / \left(U_g^J LMTD_J\right)$, where, for each section, $c_{p,g}^J$ is the average specific heat of the syngas, $T_{g,i}^J$ and $T_{g,o}^J$ are the inlet and outlet syngas temperature, $LMTD_J$ is the log mean temperature difference and U_{ht}^J is the overall heat transfer coefficient calculated from $U_g^J = \left\{\left[Nu_g k_g / d_t + \sigma F_{gt} \varepsilon_g \left(\bar{T}_g^2 + \bar{T}_t^2\right)\left(\bar{T}_g + \bar{T}_t\right)\right]^{-1} + (d_t / 2k_t) Ln[d_t/(d_t - 2t)] + (d_t - 2t)/Nu_i k_i\right\}^{-1}$. In this equation, $\bar{T}_g$ and $\bar{T}_t$ represent the average temperature for the gas and the bundles surface temperature, Nu_g, k_g, Nu_g and k_i are the Nusselt number and the thermal conductivity for the syngas and the cooling medium respectively, and d_t, t and k_t are the tube diameter, thickness and thermal conductivity for each bundle section. Table 3 shows the bundle configuration and Nusselt number expressions used in this work.

Bag filters

Cleaning of the particulate matter in the syngas is based on fabric-bag filters, specified in terms of the total inlet syngas flow rate $\dot{V}_g^{BF} = \left(\dot{H}_s^G / LHV_S^G\right) n_g^G / v_N^0$, with v_N^0 denoting the normal gas volume per unit mole, and the total electric power consumption $\dot{W}_e^{BF} = \dot{V}_g^{BF} w_e^{BF}$ where w_e^{BF} is

the specific electric power consumption, which is assumed to be constant and equal to $1.63 \cdot 10^{-3}$ kWh/Nm^3 [22]

Water gas shifting

Water Gas Shifting of the syngas is assumed to be performed in adiabatic reactor, under the assumption of having simpler designs with lower fabrication and maintenance costs. Also, adiabatic WGS leads to higher gas temperatures which allow more efficient heat recovery with lower heat transfer area. The fraction of the total syngas flow going to WGS is calculated from

$$f_{wgs} = \{[(H_2/CO)^{FT}/(H_2/CO)^{G}](\alpha_{CO}^{CC}/\alpha_{H2}^{CC}) - 1\}/\{[(H_2/CO)^{FT}/(H_2/CO)^{G}](\alpha_{CO}^{CC}/\alpha_{H2}^{CC}) + 1\} \quad (2.18)$$

where $(H_2/CO)^{FT}$ and $(H_2/CO)^{FT}$ are the H_2 to CO molar ratio after gasification but before FTS and $\alpha_{CO}^{CC}$and α_{H2}^{CC} are the outlet to inlet molar ratio of CO and H_2 in the Selexol system. The WGS process is modelled as one single overall reaction, CO (+H_2O) to CO_2 (+H_2), in presence a catalyst bed. Assuming one single operating train, dimensioning of the WGS reactor is based on the total reactor volume calculated from $V_r^{WGS} = V_{cat}^{WGS} k_v^{WGS}$ where the parameter k_v^{WGS} represents the total reactor to catalyst bed volume ratio, assumed to be 1.2 [23], and $V_{cat}^{WGS} = \left(\dot{H}_S^G / LHV_S^G\right) v_{cat}^{WGS}$ is the catalyst bed volume with v_{cat}^{WGS} calculated from

$$v_{cat}^{WGS} = f_{wgs}\{1 + x_{CO}^{G}\left(MW_{H2O}/MW_g^G\right)[(S/CO)^{WGS} - (S/CO)^{G}]\}MW_g^{WGS}\left(T_g^{WGS}/T_g^0\right)t_{cat}^{WGS} k_v^{WGS}. \quad (2.19)$$

Here, $(S/CO)^{WGS}$ is the steam to CO molar ratio required by the WGS, which is assumed to be 1.1 based on available data in the literature on the performance of commercial WGS catalysts [27], T_g^{WGS} is the average gas temperature in the WGS reactor, and $t_{cat}^{WGS}$is the residence time in the catalyst bed, assumed to be constant equal to 36 sec [24]. Considering adiabatic reactors, the

gas temperature in the WGS process must be kept below a maximum limit T_{max}^{WGS} so that the WGS reaction rate is sufficiently high to achieve complete CO conversion with short residence times. If the temperature in the WGS reactor is above T_{max}^{WGS}, a second operating reactor is required with intermediate syngas cooling between the reactors. Using the equilibrium constant for the WGS, $K_{eq}^{WGS} = \exp(-4.33 + 4557.8/T_g^{WGS})$ derived by Moe [25] for commercial catalysts and assuming $K_{eq}^{WGS} > 10$ to ensure complete CO conversion, T_{max}^{WGS} needs to be below 700 °C. Above this temperature, an additional stage is required to achieve complete WGS shifting. Dimensioning of the heat recovery boiler after the WGS reactor is based on the thermal duty $\dot{Q}_{stm}^{WGS}$ calculated from

$$\dot{Q}_{stm}^{WGS} = \left(\dot{H}_S^G / LHV_S^G\right) n_g^G f_{wgs} x_{CO}^G \bar{q}_{wgs}, \tag{2.20}$$

with $\bar{q}_{wgs} = 41.09\ kJ/mol$ denoting the heat of the WGS reaction per unit mole of CO, and $LMTD_{gw}^{WGS} = \left(T_{g,i}^{WGS} - T_{g,o}^{D}\right) Ln\left[\left(T_{g,i}^{D} - T_w^{WGS}\right)/\left(T_{g,o}^{D} - T_w^{WGS}\right)\right]$ is the logarithmic mean temperature difference. Here, T_w^{WGS} is the saturated temperature of the water in the boiler and the outlet gas temperature from the WGS reactor is estimated from $T_{g,o}^{WGS} = T_{g,i}^{WGS} + x_{g,CO} \bar{q}_{WGS} / c_{p,g}^{WGS}$ assuming a constant specific heat capacity of the gas in the reactor.

Selexol system

The Selexol system has been specified in terms of the CO_2 concentration in the syngas entering the Fischer-Tropsch synthesis, denoted by x_{g,CO_2}^{FT}. The overall CO_2 capture ratio, defined as the output to input CO_2 molar flow rate, can then be calculated in terms of the syngas composition after the EFG from

$$\alpha_{CO_2}^{CC} = \left[x_{g,CO_2}^{FT} / \left(1 + x_{g,CO_2}^{FT}\right)\right] \cdot$$
$$\left\{\left[1 - \alpha_{H_2}^{CC}\left(x_{g,H_2}^G + x_{g,CO}^G f_{WGS}\right) - \alpha_{CO}^{CC} x_{g,CO}^G (1 - f_{WGS})\right] / \left(x_{g,CO_2}^G + x_{g,CO}^G f_{WGS}\right)\right\}, \tag{2.21}$$

where $\alpha_{H_2}^{CC}$ and α_{CO}^{CC} are the capture ratios for H_2 and CO. Based on the definition of $\alpha_{CO_2}^{CC}$, the total volumetric flow rate of CO_2 capture in the Selexol system is calculated from

$$\dot{V}_{CO_2}^{CC} = \left(\dot{H}_S^G / LHV_S^G\right) v_N^0 n_g^G \alpha_{CO_2}^{CC}\, x$$

$$\left[x_{g,CO_2}^G + x_{g,CO}^G \left((H_2/CO)^{FT} - (H_2/CO)^G\right)/[1 + (H_2/CO)^{FT}]\right] \quad (2.22)$$

Dimensioning of the absorption column is based the total input flow rate of syngas and solvent, which can be calculated from in terms of the concentration of the syngas from the EFG reactor from

$$\dot{V}_g^{CC} = \left(\dot{H}_S^G / LHV_S^G\right) v_N^0 n_g^G x_{CO}^G [1 + (H_2/CO)^{FT}] \quad (2.23)$$

and

$$\dot{V}_{sel}^{ABS} = \gamma\ \dot{V}_{CO_2}^{CC} / \left(P_g^{ABS} \chi_{s-CO_2,o}^{ABS} - \gamma P_g^{FL} \chi_{s-CO_2,o}^{FL}\right) \quad (2.24)$$

where $\chi_{s-CO_2,o}^{ABS}$ and $\chi_{s-CO_2,o}^{FL}$ are the solubility of CO_2 in Selexol at the outlet of the absorber and flash tank, respectively, and $\gamma = 1.26/\left(1 - \alpha_{CO_2}^{CC}\right)^{0.07} - 0.0000138 P_g^{ABS}$ is the ratio of the actual flow ratio of Selexol relative the flow rate required to reach equilibrium. Here, we have considered a linear dependence for the selectivity of CO_2 in Selexol [26, 27] given by $\chi_{s,CO_2} = 5.26 \cdot 10^{-7} - 1.064 \cdot 10^{-8}\, T_{sel}$ based on correlations from experimental results. The temperature of the Selexol at the absorber outlet is calculated considering energy conservation for the total flow of Selexol in the absorber, giving

$$T_{s,o}^{ABS} = T_{s,i}^{ABS} + \left\{\dot{Q}_{g-s}^{ABS} + q_{sel,CO_2} \dot{V}_{CO_2}^{CC} / v_N^0\right\} / \left(\rho_{sel} c_{sel,} \dot{V}_{sel}^{ABS}\right) \quad (2.25)$$

where q_{sel,CO_2} is the heat release per unit mole of CO_2 dissolved in the Selexol, assumed to be constant and equal to 221 kJ/mole for CO_2 mass fraction in the range of 0.37–0.383 [28] and $\dot{Q}_{gs}^{ABS} = A_{gs}^{ABS} U_{gs}^{ABS} LMTD_{gs}^{ABS}$ is the total convective heat transfer from the syngas to the Selexol. Here, A_{gs}^{ABS} is the total heat transfer area from syngas to Selexol which is calculated in terms of

the volume faction of Selexol in the absorber ϕ_l^{ABS} and the Selexol droplet diameter d_{sel} from $A_{gs}^{ABS} = V_{sel}^{ABS}\phi_l^{ABS}/d_{sel}$. The heat transfer coefficient between the gas and the solvent is calculated from $U_{gs}^{ABS} = \left(k_g^{ABS}/d_p^{sel}\right)\left(2 + 0.6Re_{d_p}^{0.5}Pr^{1/3}\right)$ based on correlations from Ranz et al. [29]. Using the flow rate of Selexol from Eq. (2.28), the capture ratio for H_2 and CO can be obtained from

$$\alpha_{H_2}^{CC} = \dot{V}_{sel}^{ABS}\left(P_g^{ABS}\chi_{s-H_2,o}^{ABS} - P_g^{FL}\chi_{s-H_2,o}^{FL}\right)/\left[v_N^0\dot{N}_g^G\left(x_{g,H_2}^G + x_{g,CO}^G f_{WGS}\right)\right] \quad (2.26)$$

and

$$\alpha_{CO}^{CC} = \dot{V}_{sel}^{ABS}\left(P_g^{ABS}\chi_{s-CO,o}^{ABS} - P_g^{FL}\chi_{s-CO,o}^{FL}\right)/\left[v_N^0\dot{N}_g^G x_{g,CO}^G(1 - f_{WGS})\right] \quad (2.27)$$

where $\chi_{s-i,o}^{ABS}$ and χ_{s-i}^{FL} are the solubility of gas species in Selexol (H_2 and CO), based on the outlet conditions in the absorber and the flash tank. In this analysis, we have assumed that the solubility of both H_2 and CO is proportional to the solubility of CO_2, with a constant proportionality factor [23] equal to 0.01 and 0.028, respectively, not dependent on pressure and temperature.

2.4. FISCHER-TROPSCH SYNTHESIS AND SEPARATION

Figure 4 shows the process design for FT synthesis and separation. The syngas stream after CO_2-capture is compressed by a booster compressor and fed into the FTS reactor. The overall FTS process is here specified based on the pressure and temperature along the catalyst bed, denoted by P_r^{FT} and T_r^{FT}, the CO conversion factor γ_r^{FT} and as well the catalyst reactivity and selectivity to the different hydrocarbons products. Cooling of the FTS reactor is performed through evaporation in saturated-water tubes to achieve uniformity of the temperature inside the reactor. This avoids problems with catalyst deactivation due to sintering and coking as well as formation of significant amounts of undesirable methane in the product through methanation [30-

31]. After synthesis, waxes, with carbon number equal to or above C_{20}, are separated directly from the FTS reactor. Middle distillate and naphta, with carbon number C_{12}-C_{19} and C_5-C_{11}, respectively, are separated sequentially using water coolers. The remaining C_4 hydrocarbons and the LNG mixture, C_1-C_3, are separated based on refrigeration and cryogenic cooling, respectively. The cooling water after separation of middle distillates and naphta is used as feed water for the heat recovery system.

The total rate of energy production of each hydrocarbon C_nH_m produced from the FTS and the total thermal power production from synthesis and separation can be calculated in terms of the input power to the EFG from

$$\dot{N}_{C_nH_m}^{FT} = \left(\dot{H}_S^G / LHV_S^G\right) n_g^G \left[x_{CO}^G \left(1 - f_{wgs}\right) \alpha_{CO}^{CC} / n_{CO}^{FT}\right] w_{C_nH_m} \overline{LHV}_{C_nH_m} \tag{2.28}$$

and

$$\dot{Q}_{th}^{FT} = \left(\dot{H}_S^G / LHV_S^G\right)\left(q_r^{FTS} + q_{C_nH_m}^{SEP} + q_{pw}^{FTS}\right) \tag{2.29}$$

where $n_{CO}^{FT} = \sum_{n=1}^{N_p} \sum_m \nu_{CO} w_{C_nH_m}$ is the molar consumption of CO per unit total molar production from FTS, $\overline{LHV}_{C_nH_m}$ is the lower heating value per unit mole of C_nH_m and q_r^{FTS}, $q_{C_nH_m}^{SEP}$ and q_{pw}^{FTS} are the heat recovered from the FTS reactor, from separation of the FTS hydrocarbons and from the process water, calculated respectively from

$$q_r^{FTS} = n_g^G \left[x_{CO}^G \left(1 - f_{wgs}\right) \alpha_{CO}^{CC} / n_{CO}^{FT}\right] \sum_{n=1}^{N_p} \sum_m w_{C_nH_m} \left(\bar{h}_{C_nH_m}^f + \nu_{H_2O}^{n,m} \bar{h}_{H_2O}^f - \nu_{CO}^{n,m} \bar{h}_{CO}^f\right), \tag{2.30}$$

$$q_{C_nH_m}^{SEP} = \sum_{n=4}^{N_p} n_g^G \left[x_{CO}^G \left(1 - f_{wgs}\right) \alpha_{CO}^{CC} / n_{CO}^{FT}\right] w_{C_nH_m} \left(h_{C_nH_m}^{FT} - h_{C_nH_m}^S\right) \tag{2.31}$$

and

$$q_{pw}^{FTS} = \left[\sum_{n=1}^{N_p} \sum_m \nu_{H_2O}^{n,m} w_{C_nH_m}\right] \left(h_{sat}^{FT} - h_{pw,o}\right) \tag{2.32}$$

Here, $\bar{h}_i^f$ is the molar formation enthalpy for each species, $\nu_{H_2O}^{n,m}$ and $\nu_{CO}^{n,m}$ are the stoichiometric factors in the overall synthesis of C_nH_m, and $h_{C_nH_m}^{FT}$ and $h_{C_nH_m}^{S}$ are the thermal enthalpy of each hydrocarbon from the FTS reactor and at separation, respectively, and h_{sat}^{FT} and $h_{pw,o}$ are the thermal enthalpy of the saturated steam and outlet condensed water, respectively.

Evaluation of the product selectivity in the FTS has been described using the ASF (Anderson-Schulz-Flory) model, where the molar distribution for all the hydrocarbons with carbon number n are calculated in terms of the chain growth probability factor α, independent of n, from $\sum_m w_{C_nH_m} = n\alpha^{n-1}(1-\alpha)^2$. In this work, low-temperature FTS in a slurry phase reactor with conventional cobalt catalyst has been considered. This technology has been proven at commercial-scale to achieve up-to 80% CO conversion [32, 33], using syngas H_2/CO ratio typically in the range 1.9-2, and to maximize the production of waxes [34], which is desirable for the production of high-quality diesel fuels [35]. Co-based catalysts also exhibit high resistance to deactivation. For cobalt-based catalysts in low temperature FTS, α is assumed to be a function of the concentration of H_2 and CO and the temperature given by $\alpha = [0.633 + 0.232\, x_{CO}^{FTS}/(x_{CO}^{FTS} + x_{H2}^{FTS})][1 - 0.039(T_r^{FT} - 533)]$ based on the results from Song et al. [36]. For the production of liquid biofuels, particularly diesel-type, the factor α needs to be above 0.8 to promote formation of longer-chain hydrocarbons, which, for cobalt-based catalysts, requires temperatures in the FTS above approximately 175 °C. Dimensioning of the FTS reactor is described in terms of the total input syngas flow rate, calculated from

$$\dot{V}_g^{FT} = \left(\dot{H}_s^G / LHV_S^G\right) n_g^G v_N^0 \left[x_{CO}^G \left(1 - f_{wgs}\right) \alpha_{CO}^{CC} / \gamma_r^{FT}\right] (T_g^{FT}/T^0)(P^0/P_g^{FT}) \quad (2.33)$$

3. PLANT PROCESS ANALYSIS

Calculation of the complete process for the biocrude production plant has been performed in ASPEN PLUS using built-in models for standard equipment complemented with user-defined routines in FORTRAN for dedicated process models described in Section 2. Table 4 lists the process parameters considered in the analysis of the biocrude production plant. The analysis is performed for a reference plant capacity of 150 MW based on the input feedstock power to the EFG reactor. Tables 5 and 6 show the overall mass and energy balances for the biocrude production plant calculated for the reference plant capacity as a function of the main input parameters of the analysis, i.e., the mass fraction of the sludge in the raw feedstock, the gasification lambda value and the gasification temperature.

Dryers sizing

Figure 5 shows the variation of the thermal duty of drying agent per unit mass of evaporated water and the dryer volume per unit mass flow rate of feedstock as a function of the moisture content reduction in the dryer for feedstock particle size of 10, 15, 20 mm. The smallest particle size are here assumed to be more representative of dehydrated sludge, while the whole range are representative of the particle size after chipping of the logwood. The values for the thermal power of the drying agent are not very dependent on the particle size and are in accordance with reported results on the performance of direct-contact steam dryers [37, 38]. However, the required volume of the dryer increases both linearly with the total water evaporation and strongly with the particle size due to the reduction of the total heat transfer area and Nusselt number.

Mass and energy yields for the overall pretreatment system

Figure 6 shows the variation of the energy and mass yields for the overall pretreatment system as a function of the mass fraction of the sludge relative to the total input raw feedstock to the plant, evaluated from equations (2.7)-(2.8) and results from torrefaction experiments [13]. For all

cases, the energy yield is above 1 since the evaporation energy decrease in the drying process is greater that the energy losses due to release of combustible volatiles during torrefaction. This effect increases as the mass fraction of sludge in the raw feedstock increases. The mass yield decreases with increasing values of the torrefaction temperature due to the increased loss of combustible volatiles from the feedstock. As the fraction of sludge in the raw feedstock increases, the total mass yield decreases when the moisture content in the sludge is 80%. If the moisture content in the sludge decreases to 60%, the increase of the mass fraction of sludge in the raw feedstock is not affecting significantly the overall mass yield after pretreatment.

Operational limits for the EFG reactor

Figure 7(a) shows the operational limits of the EFG process for variable values of the mass fraction of wood relative to the total input raw feedstock. The operational limits are here represented as the variation of the S/C ratio with the lambda value for the lower and upper temperature limits. The lower temperature limit is assumed to be 1300°C in order to ensure complete ash melting [39]. The upper temperature limit is specified to be 1600°C, sufficient to achieve complete conversion of hydrocarbons to CO and H_2. The lambda value is considered to be within the range of 0.2-0.4 [40]. The S/C ratio is then calculated within the lambda value range to achieve the upper and lower temperature limits. As shown in Figure 7(a), the S/C ratio increases linearly with increasing lambda value for all cases. For constant lambda value, the required steam amount increases with increasing fractions of the woody biomass relative to organic waste, due to the higher calorific value of the former, and decreases with the gasification temperature. Figure 7(b) shows the variation of the H_2 to CO molar ratio of the syngas leaving the EF gasification for the operational limits. These results show that lower gasification temperatures lead to higher H_2/CO molar ratio. This figure also shows that increasing values of the mass fraction of sludge leads to

higher H_2/CO ratios, this effect being stronger at lower temperatures and lambda values. This can be explained due to the higher H/C ratio of the organic waste as compared to woody biomass.

Cold-gas efficiency and output thermal power of the EFG process

Figure 8 shows the variation of the (a) cold-gas efficiency and (b) the output thermal energy per unit feedstock energy in the EFG process as a function of the lambda value for variable values of the mass fraction of wood relative to the total input raw feedstock, evaluated from

$$\epsilon_{cg}^{G} = n_{g}^{G} x_{g,,CO}^{G} \left[\overline{LHV}_{CO} + \overline{LHV}_{H_2} (H_2/CO)^{G} + \sum \left(x_{g,,i}^{G} \, \overline{LHV_i} \right) / x_{g,,CO}^{G} \right] / LHV_{s}^{G} \quad (3.1)$$

and

$$\epsilon_{th}^{G} = n_{g}^{G} x_{g,,CO}^{G} \left[\bar{c}_{p,CO} + \bar{c}_{p,H_2} (H_2/CO)^{G} + \sum \left(x_{g,,i}^{G} \, \bar{c}_{p,i} \right) / x_{g,,CO}^{G} \right] \left(T_{g}^{G} - T^{0} \right) / LHV_{s}^{G}, \quad (3.2)$$

where $\overline{LHV}_i$, $\bar{c}_{p,i}$ and $x_{g,,i}^{G}$represent the molar low heating value, specific heat and concentration for each molecular species at the EFG reactor outlet. The cold gas efficiency decreases linearly with the lambda value, due to increase combustion of the gas, and with decreasing values of the mass fraction of wood in the raw feedstock. This can be explained since the sludge has significantly higher ash content as compared to the wood, which decreases the total mass flow rate of syngas. The output thermal energy increase linearly with lambda value, the rate of increase being higher with higher mass fraction of wood in the raw feedstock.

Biocrude and LNG production efficiency

The net production efficiency of biocrude and LNG, here defined respectively as the mixture of hydrocarbons from FTS with carbon number above 3 and between 1 and 3, are calculated relative to the input feedstock power to the EFG from

$$\epsilon_{bc} = (\overline{LHV}_{bc} / LHV_{S}^{G}) n_{g}^{G} \left[x_{CO}^{G} \left(1 - f_{wgs} \right) \alpha_{CO}^{CC} / n_{CO}^{FT} \right] \quad (3.3)$$

and

$$\epsilon_{LNG} = (\overline{LHV}_{LNG}/LHV_S^G) n_g^G \left[x_{CO}^G \left(1 - f_{wgs}\right) \alpha_{CO}^{CC}/n_{CO}^{FT}\right] \quad (3.4)$$

where $\overline{LHV}_{bc} = \sum_{n=4}^{N_p} \sum_m w_{C_nH_m} \overline{LHV}_{C_nH_m}$ and $\overline{LHV}_{LNG} = \sum_{n=1}^{3} \sum_m w_{C_nH_m} \overline{LHV}_{C_nH_m}$ are the molar lower heating value of the biocrude and the LNG, respectively. Figure 9 shows the variation of the efficiency for the biocrude (a) and LNG (b) power production relative to the input biomass power to the gasification unit, calculated from equations (7.3)-(7.4), as a function of the lambda value in the EFG for wood to sludge mass ratio of 100, 75 and 50%. In general, the biocrude and LNG production decreases with increasing values of the gasification lambda value due to increased oxidation of the syngas. With increasing fraction of sludge in the input feedstock, the biocrude production decreases due to the lower carbon content in the sludge compared to the wood. However, the influence of the gasification temperature on the biocrude production exhibit different trends depending on the input feedstock composition. For 100% wood, the biocrude production decreases with increasing temperatures in the EFG for equivalence ratios lower than approximately 0.25, but this trend becomes opposite as the equivalence ratio increases above approximately 0.30. This opposite trend of the biocrude production with EFG temperature disappears as the sludge fraction in the feedstock increases above 25%, where lower values of the EFG temperature lead to higher biocrude power production.

Heat balance for the overall plant

The net thermal power production for the overall plant is calculated from

$$\boldsymbol{\epsilon_{th}} = (1/LHV_S^G)\left(q_{th}^{GCC} + q_{th}^{FTS} + q_{pw}^{GCC} + q_{pw}^{FTS} - q_g^{PR}\right) \quad (3.5)$$

where all the heat terms inside the second parenthesis are per unit feedstock energy input to the EFG. Here, $q_{th}^{GCC} = q_g^{GCC} - q_{stm}^{GCC}$ represents the net heat recovered from gasification and syngas cooling and conditioning, where $q_g^{GCC} = n_g^G \left[\bar{c}_{p,g}^G \left(T_g^G - T_g^{CC}\right) + f_{WGS} x_{CO}^G \bar{q}_{wgs}\right]$ is the thermal

energy recovered from the syngas cooling and conditioning and $q_{stm}^{GCC} = \{(S/C)_g n_{s,C} - y_{S,H_2O}^G/W_{H2O} - n_g^G f_{WGS} x_{CO}^G[(S/CO)^{WGS} - x_{H2O}^G/x_{CO}^G]\}(\bar{h}_{stm}^{sat} - \bar{h}_w^0)$ is the steam energy required by gasification and WGS, $q_{th}^{FTS} = q_r^{FTS} + q_{C_nH_m}^{SEP}$ is the net heat recovered from Fischer Tropsch synthesis and separation with q_r^{FTS} and $q_{C_nH_m}^{SEP}$ denoting the thermal energy recovered from the FTS process and from separation of FTS products calculated from Equations (2.30) and (2.31), $q_{pw}^{GCC} = n_g^G[x_{H2O}^G(1 - f_{WGS}) - f_{WGS} x_{CO}^G (S/CO)^{WGS}](h_{sat}^{GCC} - h_{pw,o})$ is the heat recovered from process water from gasification and syngas cooling and conditioning, q_{pw}^{FTS} is the heat recovered from the process water in the Fischer Tropsch and separation system calculated from Equation (2.32), and $q_g^{PR} = \sum(Y_j^F q_j^{PR})$

is the total heat consumed by the overall pretreatment system, with $q_j^{PR} = (\Delta h_g^D/h_{g,i}^D)[\Delta y_{j,H_2O}^{PR}(h_{H2O}^v + h_{g,o}^D) + c_{j,s}\Delta T_s^{PR}] - (1 - y_{j,H_2O}^F)[LHV_{j,dry}^F - (1 - \Delta y_{j,v}^{PR})LHV_{j,dry}^{PR}]$ denoting the heat consumed for each feedstock.

Table 7 shows the main heat flows for the biocrude production plant calculated for the reference plant capacity as a function of the main input parameters of the analysis, i.e., the mass fraction of the sludge in the raw feedstock, the gasification lambda value and the gasification temperature. Figure 10 shows the variation of the net thermal power production relative to the input biomass energy flow to the gasification unit, calculated from equation (3.7), as a function of the operating conditions in the EFG reactor and the raw feedstock composition, for a steam temperature in the dryers equal to 150 (a) and 200 °C (b). The moisture content in the input raw wood and sludge to the plant has been assumed to be 50 and 60% respectively. Operating the EFG in the upper temperature limit, the net thermal power production exhibits a general monotonic increase with the lambda value in the EFG due to increased combustion of the syngas, which leads to increased

steam production from the syngas cooling. In the lower temperature limit in the EFG, the net thermal power decreases with the equivalence ratio due to increased consumption of steam in the gasification. With increasing fraction of sludge in the input feedstock, the net thermal production reduces significantly due to higher heat requirement for drying the sludge compared to the wood. When using steam at 150 °C for drying and operating the EFG at the lower temperature limit, the net production of heat from the syngas cooling, conditioning and synthesis approximately equals the heat requirement for the feedstock pretreatment. Increasing the steam temperature in the dryers reduces the heat consumption for pretreatment leading to positive net thermal production for the overall plant.

4. PLANT ECONOMICS

The economic performance of the biocrude production plant has been evaluated in terms of the capital and operating costs and the total cost of biocrude production. The results are presented for plant scales in the range of 150-600 MW, based on the input feedstock power to the EFG system, and as a function of the composition of the input raw feedstock.

4.1. CAPITAL COST

The capital cost of the plant has been evaluated in terms of the total permanent investment, which is calculated from

$$C_{TPI} = \left(\sum_i C_{P,k}\right)\left[1 + f_{site} + f_{building} + f_{land}\right]\left[1 + f_{cont} + f_{eng}\right]\left[1 + f_{dev} + f_{com}\right], \quad (4.1)$$

where $C_{P,K}$ is the total purchase and installation cost for a specific equipment k, and f_i represents additional costs factors including civil work associated with site preparation and process-equipment building, offsite accessibility and services, contingency margin, contractors, land, royalties and patents. Representative values for f_i [41, 42] are listed in Table 8.

Equipment purchase and installation costs have been calculated using a modification of the base-cost method proposed by Guthrie-Ulrich [42], given by

$$C_{P,k} = N_t C_{p,I_b}(I/I_b) f_P f_{mat} f_{BM} f_{inst} k_t^{N_t}, \quad (4.2)$$

where $C_{p,I_b}(S/N_{t,op})$ is the equipment purchase cost calculated as a function of the actual equipment size S_k and the number of operating units $N_{t,op}$ at the cost index I_b related to a reference year, N_t is the total number of units, I is the cost index for the actual year, f_{mat} and $f_P = (P/P_b)^{k_p}$ are factors accounting for a different material and pressure than the one considered in the purchase cost function C_{p,I_b}, with k_p being assumed to be constant and equal to 2.208 [26], f_{inst} is the installation factor, f_{BM} is the bare module factor which accounts for the cost of auxiliary equipment and piping associated to the main equipment, and $k_t^{N_b}$ is the train cost factor [43] where the parameter k_t is assumed to be constant and equal to 0.9 [44]. The train cost factor considers that the cost of multiple units reduces due to share of auxiliaries and installation costs. The cost index used in this study is based on the Chemical Engineering Plant Cost Index (CEPCI). Values for f_{inst} are based on individual installation factors per type of process equipment developed by Woods [45] with an updated labor correction factor under Norwegian conditions of 1.47.

The purchase cost functions for the main process equipment that has been considered in this work are based on data published by the authors in a previous work [12], with modifications as presented below. The cost of feedstock storage at the plant is calculated from $C_P^{ST} = \sum_J c_{J,st}\, \dot{M}_J^F t_{st}/\rho_J$, where t_{st} is the storage time capacity, assumed to be one week, and $c_{J,st}$ is the storage cost per unit volume, which is assumed to be constant and equal to 5.3 €/m^3 not dependent on the type of feedstock. The purchase cost of the direct-contact steam dryers (M$) has been estimated in terms of the total surface area of the drier A_r^D using the cost function $C_p^D =$

$2.55(A_s)^{0.6}$ based on industrial data. The purchase cost of the torrefaction reactor is evaluated as a function of the volume from the correlation $C_p^T = 5.1(V_r^T/100)^{0,735}$ obtained from the reported values [47] of 5.65 and 6.70M$ for 115 and 145 m^3 reactor volume, respectively. Purchase cost of the bag filter house is $C_p^{BF} = 1.1(\dot{V}_g^{WGS}/50000)^{0.798}$. Purchase cost of the cryogenic unit for the LNG is evaluated based on the input normal flow rate from $C_P^{LNG} = 9.1(\dot{V}_{N,g}^{LNG}/765)^{0.7}$. Figure 11 shows the total permanent investment as a function of the feedstock input power to the EFG of a) the overall pretreatment system for variable fraction of wood in raw feedstock and b) the gasification and syngas cooling and conditioning and the Fischer Tropsch and separation systems. As shown in Figure 11, increasing the amount of sludge in the raw feedstock has a different effect on the investment cost depending on the plant scale. For smaller scales below 200 MW, co-processing sludge lead to an increase in the total capital cost of pretreatment relative to pretreating 100% wood due to a dominant effect of the additional investment in driers, conveyors and grinding. Increasing the fraction of sludge reduces this effect due to smaller the size of the pretreatment train of the wood. For higher plant scales, above 200 MW, co-processing sludge lead to lower investment cost due to lower scale factor for the pretreatment train of sludge compared to the wood. Figure 12 shows the variation of the specific capital cost of the biocrude production plant as a function of the plant scale and the composition of the input raw feedstock to the plant. The plant specific capital cost is here defined as the total permanent investment divided by the input feedstock power to the EFG. The moisture content of the wood and the sludge are assumed to be 50 and 80%, respectively, which correspond to the upper values in the specified range. For each plant capacity, the capital cost for the gasification, cooling and conditioning system and for the FTS and separation system are constant and equal to the maximum values based on the process parameters specified in Table 8, while the capital cost

for the pretreatment varies with the composition of the input feedstock. These results shows an increase in the specific capital cost of the plant with increasing mass fraction of sludge in the raw feedstock, due to the higher moisture content of the sludge which requires larger drying capacity and thus higher capital cost for the pretreatment system.

4.2. OPERATING COST

The total operating cost for the biocrude production plant is calculated per annual basis from

$$C_{PROD} = C_F + C_{op,d} + C_{op,i} + C_{maint}, \quad (4.3)$$

where C_F is the total cost of feedstock supply, $C_{op,d}$ represents the variable direct operational cost dependent on the annual processing of feedstock, $C_{op,i}$ are the fixed indirect operational costs required for having the plant in activity, and C_{maint} are the maintenance costs.

Feedstock supply cost

The total cost of supply feedstock is then calculated from

$$C_F = \sum_J \left(\dot{M}_J^F t_{prod}/\rho_J\right)\left[c_{J,pr} + c_{J,tr-f} + c_{J,tr-L} L_J\right] \quad (4.4)$$

where t_{prod} is the annual production time, ρ_J is the raw feedstock density, $c_{j,pr}$ is the feedstock production cost per unit volume and $c_{J,tr-f}$ and $c_{J,tr-L}$ are the fixed and distance-dependent transport costs per unit volume. The average feedstock transport distance is here estimated from $L_J = 2\left(\dot{M}_J^F T_{prod}/m_{J,S}\right)^{1/2}$ where $m_{J,S}$ is the feedstock availability per unit area. Table 9 shows the assumed values for biomass density, annual production and unit costs under Norwegian conditions [48]. In equation (4.4), $\dot{M}_J^F$ is the total mass flow rate of each raw feedstock supplied to plant, which is calculated in terms of the total input power to the EFG $\dot{H}_{in}^G$ from

$$\dot{M}_J^F = Y_j^F \dot{H}_S^G / \sum\left(Y_j^F NCV_{s,j}^F \epsilon_j^{PR}\right) \quad (4.5)$$

where Y_j^F is the mass fraction of the feedstock and ϵ_j^{PR} is the overall energy yield after pretreatment of the feedstock. Figure 13 shows the variation of the cost of feedstock supply per unit feedstock input power as a function of moisture content in the input wood and for sludge to wood mass ratio equal to 0, 0.25 and 0.5 and for a gate fee of the sludge at source of 0 and 10$/ton. It has been assumed that the sludge is produced at one location at a distance of 100 km from the plant while the wood is uniformly distributed around the plant. The cost of feedstock supply is strongly dependent on the gate fee (negative production cost) of sludge. As the gate fee increases from zero to 10 $/ton, the cost of feedstock supply decreases approximately by 35% when increasing the fraction of sludge to 50%.

Direct operational costs

Evaluation of the direct operational cost are evaluated from

$$C_{op,d} = C_{chem} + C_{em} + C_{res} + C_{ef} + C_{fw}, \quad (4.6)$$

where C_{chem}, C_{em}, C_{res}, C_{ef}, C_{fw} are annual cost of chemicals, emissions to air, disposal of solid residues, treatment and disposal of effluents and supply of fresh water, calculated based on individual rates of consumption or production obtained from the mass and energy balances, the unit cost values of each specific item, and the plant annual operating time. The costs of catalyst consumption are estimated from $C_{cat}^J = n_{cat}^J \left(\dot{V}_g^J c_{cat}^J\right)/\left(1/\tau_{cat}^J\right)$ with J denoting the WGS and FT reactors, $\dot{V}_g^J$and $1/\tau_{cat}^J$ representing the volumetric gas flow rate and the characteristic space velocity in the catalyst bed, respectively, c_{cat}^J denoting the unit cost of catalyst per unit volume and n_{cat}^J denoting the catalyst replacements per year or aging factor. Volume is sized by assuming constant gas hourly space velocity (GHSV) of 100 per hour for both WGS and FT catalysts respectively [24]. One catalyst bed replacement after the first operating year is

assumed, and then replacement every three years after that. Physical solvent (Selexol) is the only consumable for gas cleaning that has been considered in this work, the associated cost being estimated from $C_{chem}^{GC} = n_{sel}\dot{V}_{sel}^{CC}\rho_{sel}c_{sel}\tau_{sel}$, where $\dot{V}_{sel}^{CC}$ is the flow rate of Selexol, τ_{sel} is the total residence time of Selexol in the gas cleaning system, n_{sel} is the number of Selexol replacements per year and c_{sel} is the cost per unit mass of Selexol. Table 10 summarizes the reference unit values for the direct operational costs considered in this work.

Indirect operational costs

The annual indirect operational costs have been evaluated from

$$C_{op,i} = C_{labor} + C_{adm} + C_{insur} + C_{tax}, \quad (4.7)$$

where C_{labor}, C_{adm}, C_{insur} and C_{tax} are, respectively, labour, administration, insurance and taxes. The total annual labor cost C_{labor} has been estimated from

$$C_{labor} = c_{r,h}\sum_j N_j\left[f_{r,j}(1 + f_{lb}) + f_{OH,j}c_{OH}\right] \quad (4.8)$$

where $c_{r,h}$ denotes the average hourly rate in Norway, the subscript j denotes the personnel categories, and N_j, $f_{r,j}$, f_{lb}, $f_{OH,j}$ and c_{OH} represent the annual man-hour of personnel required, the hourly rate factor, the labour burden factor, the overhead factor and the overhead cost factor, respectively. In this work, the personnel categories considered are regular operator, skilled operator and lab technician. The number of personnel required has been estimated based on individual main systems, i.e. feedstock pretreatment, syngas production and cooling, gas cleaning and conditioning, FT synthesis and separation, air separation unit and process water treatment areas. It is assumed that each area requires equal number of personnel per category, two regular operators, one skilled operator, one foreman and two lab technicians. Table 11 provides the values for labor cost parameters considered in Equation (4.8) according to Norwegian conditions. This work only considers overhead for regular and skilled operators

associated to unplanned plant shutdowns due to equipment failures. Costs for administration and insurance are evaluated as a percentage of the total permanent investment according to Table 5. The taxes for net plant income are evaluated based on standard tax rate of 28 % in accordance to company tax law and additionally 2% inflation are also accounted for.

Maintenance cost

The annual maintenance cost has been calculated from

$$C_{maint} = t_{prod}\left[c_{spares} + c_{shut}f_{shut}\right], \quad (4.9)$$

where t_{prod} is the plant annual production time, c_{spares} is overall cost of spare parts, including procurement, storage and replacement, per unit time of operation, c_{shut} and f_{shut} denotes the cost per unit time and the fraction of the total annual production time associated to unplanned shutdowns. This work has assumed that the total cost of spare parts is proportional to the total purchase and installation cost, $t_{prod}c_{spares} = f_{spares}\sum_i C_{S,I,i}$, where f_{spares} is a constant proportionality factor equal to 2%. The unit cost for shutdown c_{shut} is calculated as the net annual income divided by the planned annual hours of operation of the plant and f_{shut} is assumed to be also constant and equal to 2%.

Table 12 shows the distribution of the annual direct and indirect operating costs per unit biocrude energy produced ($/GJ) for a base plant capacity of 150 MW for mass fraction of wood in the feedstock of 100, 75 and 50%. The major contributors to the annual operating costs are biomass feedstock, labor cost and maintenance which, for 100% of wood, contribute approximately 34, 22 and 18% of the total annual operating costs. As the gate fee of sludge increases, the feedstock supply cost decreases significantly.

4.3. COST OF BIOCRUDE

The cost of biocrude, here defined as the average biocrude price per unit energy produced required so that the overall net present value (NPV) of the plant over its lifetime becomes zero, is calculated from

$$C_{biocrude} = \sum_{i=1}^{N} \left[\frac{(C_{TPI,i}+C_{PROD,i})-C_{COP,i}}{(1+r)^i}\right] / \sum_{i=1}^{N} \left[\frac{t_{prod,i}\dot{H}_{bc}}{(1+r)^i}\right] \quad (4.10)$$

where r is the expected return of investment, $C_{TPI,i}$, $C_{PROD,i}$ and $C_{COP,i}$ are, respectively, the distribution of the annual total investment, the operating cost and income from co-products over the plant life time. The co-products considered are the exported heat and the CO_2 credits. The financial assumptions and the values for co-products in the Norwegian market are shown in Table 13. All the plant costs are updated to 2016 CEPCI index. Figure 14 shows the variation of the cost of biocrude as a function of the plant scale, the raw feedstock composition and the gate fee for the sludge. The moisture content of the wood and the sludge are assumed to be 50 and 80%, respectively. The plant capital cost correspond to the values shown in Figure 12. Considering 100% wood as a reference case, the cost of biocrude production ranges between 32 and 30 $/GJ. As the fraction of sludge increases, the cost of biocrude is very dependent on the gate fee. For zero cost of sludge at source, the cost of biocrude is above the reference values obtained by considering 100% wood and increases with the fraction of sludge. In this case, the increase of investment in pretreatment for treating the sludge becomes dominant compared to the lower feedstock cost obtained by increasing the fraction of sludge in the raw feedstock. As the gate fee increases, above approximately 12 $/ton, the reduction in feedstock supply cost by increasing the fraction of sludge has a dominant effect compared to the higher investment cost for pretreatement, which leads to lower cost of biocrude. For a gate fee of about 50$/ton and a mass fraction of sludge in the raw feedstock of 50 %wt., the cost of biocrude is in the range of

23-25 $/GJ for plant capacities in the range of 150-600 MW based on the input feedstock energy to the EFG.

5. CONCLUSIONS

Co-processing sludge residues from anaerobic digestion with woody biomass in an entrained flow gasification has been proven to improve the overall cost of biocrude production from Fischer-Tropsch synthesis when considering gate fees for the sludge above 20 $/ton. For this gate fee, although the sludge has lower calorific value and higher moisture, which require higher capital investment for pretreatment, the reduction of feedstock supply cost with increasing fraction of sludge becomes dominant in evaluating the overall cost of production. For gate fees of 50 $/ton, which are realistic for the current waste market, the cost of biocrude ranges between 18 and 22 $/GJ for plant scales between 150 and 600 MW based on the input feedstock energy to the entrained flow gasifier. Moreover, the overall efficiency for biocrude and LNG production, and therefore the main income to the plant, is comparable for mass fractions of the sludge in the raw feedstock ranging between 0 and 50%. Based on direct-contact superheated steam dryers for the pretreatment of sludge, the residual heat recovered from the main conversion process is sufficient to co-process up to 50% mass fraction of sludge in the raw feedstock with moisture content of 80%. The parametric results presented in this work can be integrated in wider mathematical models to evaluate the economic performance of liquid biofuels production in a value chain perspective. Moreover, the parameterization approach allows a probabilistic analysis the biocrude production plant, particularly to evaluate how uncertainties and variabilities affect the economic performance. This analysis will be the subject of future work by the authors.

Acknowledgement: The authors gratefully acknowledge the financial support from the Research Council of Norway and the industry partners Silva Green Fuel AS, Avinor, Viken Skog AS, ECOPRO AS and CAMBI ASA through the project GAFT (Gasification and FT-Synthesis of Lignocellulosic Feedstocks) to perform this work.

References

[1] Ribeiro, K.; Kobayashi, S.; Beuthe M.; Gasca, J.; Greene, D.; D. S. Lee, D. S.; Muromachi, Y.; Newton, P. J.; Plotkin, S.; Sperling, D.; Wit, R.; Zhou, P. J. *Transport and its infrastructure. In Climate Change 2007: Mitigation. Contribution of Working Group III to the Fourth Assessment Report of the Intergovernmental Panel on Climate Change*; Cambridge University Press: 2007.

[2] Transport energy consumption and emissions – Statistics Explained. EUROSTAT: Luxembourg;.http://epp.eurostat.ec.europa.eu/statistics_explained/index.php/Transport_energy_consumption_and_emissions.

[3] Greenhouse Gas Inventory Data Explorer, Environmental Protection Agency; https://www3.epa.gov/climatechange/ghgemissions/inventoryexplorer/index.html#transportation/allgas/source/all

[4] The Norwegian scenario and action plan presented by NITO Future Climate - Engineering solutions. NITO: Oslo, 2009; p 41; http://www.fc-es.net/wp-content/themes/fces/uploads/2012/08/National-Climate-Plan-Norway-Phase-1.pdf.

[5] A Roadmap for moving to a competitive low carbon economy in 2050, European Commission: Brussels, 2011; http://eur-lex.europa.eu/LexUriServ/LexUriServ.do?uri=COM:2011:0112:FIN:en:PDF

[6] Sims, R. E. H.; Mabee, W.; Saddler, J. N.; Taylor, M. An overview of second generation biofuel technologies. *Bioresour. Technol.* **2010**, 101 (6), 1570−1580.

[7] Nordic Energy Technology Perspectives, Pathways to a Carbon Neutral Energy Future: OECD/IEA, Paris, 2013.

[8] Zhou, J.; Chen, Q.; Zhao, H.; Cao, X.; Mei, Q.; Luo, Z.; Cen, K. Biomass–oxygen gasification in a high-temperature entrained-flow gasifier *Biotechnology Advances*, **2009**, 27(5), 606–611

[9] Hernandez, J. J.; Aranda-Almansa G.; Bula, A. Gasification of biomass wastes in an entrained flow gasifier: Effect of the particle size and the residence time. *Fuel Processing Technology*, **2010**, 91, 681-92.

[10] Swanson, R. M.; Platon, A.; Satrio, J. A.; Brown, R. C. Techno-economic analysis of biomass-to-liquids production based on gasification. *Fuel* **2010**, 89 (Supplement 1, (0)), S11−S19.

[11] Boerrigter, H. *Economy of Biomass-to-Liquids (BTL) plants: an engineering approach*, ECN Report, No. ECN-C--06-019, 2006.

[12] Kempegowda, .R S. ; del Alamo, G.; Berstad, D.; Bugge, M.; Matas-Güell B.; Tran, K.Q. CHP-integrated Fischer-Tropsch biocrude production under Norwegian conditions: techno-economic analysis. *Energy & Fuels*, **2015**, 29 (2), 808-822

[13] Tapasvi, D.; Khalil, R.; Skreiberg, Ø.; Tran, K.-Q.; Grønli, M., Torrefaction of Norwegian Birch and Spruce: An Experimental Study Using Macro-TGA. *Energy & Fuels,* **2012**, 26 (8), 5232-5240.

[14] Laitila, J.; Asikainen, A.; Ranta, T.; Cost analysis of transporting forest chips and forest industry by-products with large truck-trailers in Finland. *Biomass and Bioenergy*, **2016**, 90, 252-261.

[15] Spinelli, R.; Cavallo, E.; Eliasson, L.; Facello, A., Comparing the efficiency of drum and disc chippers. *Silva Fennica*, **2013**, 47(2), 1-11

[16] Kuwahara, F.; Shirota, M.; Nakayama, A. A numerical study of interfacial convective heat transfer coefficient in two-energy equation model for convection in porous media. *International Journal of Heat and Mass Transfer*, **2011**, 44, 1153-1159

[17] Govin, A.; Repellin, V.; Rolland, M.; Duplan, J. L. Effect of torrefaction on grinding energy requirement for thin wood particle production. Nicolas Roche. XII° Congrès de la Société Française de Génie des Procédés Pour relever les défis industriels du XXI° siècle, Marseille, Oct. 2009

[18] Arnold, K.; Stewart, M., *Surface Production Operations: Design of Gas-Handling Systems and Facilities, Vol. 2.* Gulf Professional Publishing: 1999

[19] Frey, H.C.; Akunuri,, N. *Probabilistic Modeling and Evaluation of the Performance, Emissions, and Cost of Texaco Gasifier-based Integrated Gasification Combined Cycle Systems using ASPEN [software]*. Raleigh, NC: North Carolina State University, January 2001.

[20] Khan, W. A.; Culham, J. R.; Yovanovich, M. M., Optimal Design of Tube Banks in Crossflow Using Entropy Generation Minimization Method. 44th AIAA Aerospace Sciences Meeting and Exhibit, 9 - 12 January 2006, Reno, Nevada

[21] Incropera F. P., *Fundamentals of Heat and Mass Transfer*. Wiley and Sons, 2006.

[22] Stubenvoll, J.; Böhmer, S.; Szednyj, I., *State of the Art for Waste Incineration Plants.* Austrian Federal Ministry of Agriculture and Forestry. Vienna, 2002. http://www.umweltbundesamt.at/fileadmin/site/umweltthemen/industrie/pdfs/english_version.pdf

[23] Chen, C. A Technical and Economic Assessment of CO_2 Capture Technology for IGCC Power Plants; Carnegie Mellon University: 2005.

[24] Swanson, R. M.; Platon, A.; Satrio, J. A.; Brown, R. C., Techno-economic analysis of biomass-to-liquids production based on gasification. *Fuel*, **2010**, 89, Supplement 1, (0), S11-S19.

[25] Moe J. M., Design of water-gas shift reactors, *Chemical Engineering Progress*, **1962**, 58, 33-36

[26] Black W. B.; Pritchard V.; Holiday A.; Ong J. O.; Sharp C., Use of SELEXOL Process in Coke Gasification to Ammonia Project. Laurance Reid Gas Conditioning Conference at the University of Oklahoma, 2000, Norman, Oklahoma

[27] Doctor R.D., KRW oxygen-blown gasification combined cycle carbon dioxide recovery, transport, and disposal. Report ANL/ESD-34, Argonne National Laboratory, 1996

[28] Tsunatu, D. Y.; Mohammed-Dabo, I. A.; Waziri, S. M., Technical Evaluation of Selexol-Based CO_2 Capture Process for a Cement Plant. *British Journal of Environment & Climate Change,* **2015**, 5(1), 52-63

[29] Ranz, W.; Marshall, W., Evaporation from drops. *Chem. Eng. Prog*. **1952**; 48: 141–146.

[30] Wender, I., Reactions of synthesis gas. *Fuel Processing Technology,* **1996**, 48 (3), 189-297.

[31] Schulz, H., Short history and present trends of Fischer–Tropsch synthesis. *Applied Catalysis A: General*, **1999**, 186, (1–2), 3-12.

[32] Bridgwater, A., *Progress in thermochemical biomass conversion*. John Wiley & Sons: 2008.

[33] Ouwens, D.; den Uil, C.; Boerrigter, H., Tri-generation from biomass and residues: Options for the co-production of Fischer-Tropsch liquids, electricity and heat. *Proceedings of Progress in thermodynamical biomass conversion (PITBC)*, Tyrol, Austria, **2000**, 17-22.

[34] Rytter, E.; Ochoa-Fernández, E.; Fahmi, A., Biomass-to-Liquids by the Fischer–Tropsch Process. *Catalytic Process Development for Renewable Materials, E*d. Wiley-VCH Verlag GmbH & Co. Weinheim, Germany 2013, 265-308.

[35] Dry, M. E., The Fischer–Tropsch process: 1950–2000. *Catalysis Today*, **2002**, 71, (3–4), 227-241.

[36] Song, H.; Ramkrishna, D.; Trinh, S.; Wright, H. Operating Strategies for Fischer-Tropsch Reactors: A Model-Directed Study. *Korean Journal of Chemical Engineering*, **2004**, 21(2), 308-317

[37] Amos, W.A. *Report on Biomass Drying Technology*. NREL/TP-570-25885. Golden, CO: National Renewable Energy Laboratory, November 1998. http://www.nrel.gov/docs/fy99osti/25885.pdf

[38] Li, H.; Chen, Q.; Zhang, X.; Finney, K.N.; Sharifi, V.N.; Swithenbank J., Evaluation of a biomass drying process using waste heat from process industries: A case study. *Applied Thermal Engineering*, **2012**, 35, 71–80

[39] Olanders, B.; Steenari, B.-M., Characterization of ashes from wood and straw. *Biomass and Bioenergy*, **1995**, 8 (2), 105-115

[40] Qin, K.; Jensen, P. A., Lin, W., Jensen, A. D., Biomass Gasification Behavior in an Entrained Flow Reactor: Gas Product Distribution and Soot Formation. *Energy & Fuels*, **2012**, 26 (9), 5992-6002

[41] Peters, M. S.; Timmerhaus, K. D.; West, R. E.; Timmerhaus, K.; West, R., *Plant design and economics for chemical engineers,* Vol. 4.. *5th ed*., McGraw-Hill New York: 2003,

[42] Ulrich, G. D.; Vasudevan, P. T., Chemical engineering process design and economics: a practical guide. Process Pub.: 2004.

[43] Martelli, E.; Kreutz, T.; Carbo, M.; Consonni, S.; Jansen, D., Shell coal IGCCS with carbon capture: Conventional gas quench vs. innovative configurations. *Applied Energy,* **2011**, 88 (11), 3978-3989

[44] Larson, E. D.; Jin, H.; Celik, F. E., Large-scale gasification-based coproduction of fuels and electricity from switchgrass. *Biofuels, Bioproducts and Biorefining*, **2009**, 3(2), 174-194

[45] Woods, D. R., *Rules of Thumb. Rules of Thumb in Engineering Practice*. Wiley-VCH: 2008

[46] Ereev, S..; Patel, M. Recommended methodology and tool for cost estimates at micro level for new technologies. Utrecht, October 2011. http://www.prosuite.org/c/document_library/get_file?uuid=0efb1401-9854-4b92-8741-b0955c387cfa&groupId=12772

[47] Bergman, P.C.A.; Boersma, A.R.; Zwart, R.W.R.; Kiel, J.H.A., Torrefaction of biomass for co-firing in existing coal-fired power stations. ECN Report ECN-C-05-013, July 2005. https://www.ecn.nl/docs/library/report/2005/c05013.pdf

[48] Trømborg, E.; Havskjold, M.; Lislebø, O.; Rørstad, P. K., Projecting demand and supply of forest biomass for heating in Norway. *Energy Policy*, **2011**, 39 (11), 7049-7058.

Tables and Figures

Table 1: Measured feedstock properties (Proximate and ultimate analysis, heating values and yields) for raw Norwegian stem wood, bark and top and branches from spruce [13] and sludge from anaerobic digestion. The measured composition of the sludge was based on samples provided by one of the industrial partners participating in the project

Feedstock	Woodchips (spruce)	Stem wood (spruce)	T&B (spruce)	Bark (spruce)	Sludge from anaerobic digestion
Volatiles (% wt. dry)	79.97	72.43	69.82	70.62	14.93
Fixed Carbon (% wt. dry)	19.65	27.27	24.49	26.85	50.74
Ash (% wt. dry)	0.38	0.30	5.69	2.53	34.34
HHV (MJ/kg dry)	20.13	19.90	19.94	20.25	15.28
C (% wt. dry)	48.78	47.38	51.53	49.09	33.58
H (% wt. dry)	6.27	6.4	6.51	6.06	5.06
O (% wt. dry)	44.8	46.1	41.5	44.38	56.24
N (% wt. dry)	0.13	0.09	0.44	0.45	4.24
S (% wt. dry)	0.01	0.01	.02	0.02	0.88
Cl (% wt. dry)	0.00	0.002	0.04	0.02	0.19

Table 2: Particle size distribution from drum chipper, based on experimental data from Laitila et al. [14]

Particle size (mm)	>45	16-45	8-16	1-8	<1
Mass fraction (%)	0.7	3.4	63.7	29.2	3

Table 3: Nusselt numbers used for calculating the convective heat transfer coefficient from the syngas to the cooling medium for each section of the syngas cooling train, where Re_{dt} represents the Reynolds number based on the average cross section velocity and the tube dimeter in each section [20,21]

Section of the cooling train	Bundle configuration	Syngas side Nusselt Number
Radiation chamber	Vertical tubes	$Nu_{d_t}^{PF} = Re_{d_t}^{0.8} Pr^{1/3}(0.026(S/d_t) - 0.006)$
Evaporator, super-heater and economizer	Horizontal, staggered tubes	$Nu_{d_t}^{CF} = Re_{d_t}^{1/2} Pr^{1/3} \left(0.61 {S_T}^{0.091} {S_L}^{0.091}\right)/[1 - 2\exp(-1.09 S_T)]$
Smoke tube boiler	Vertical tubes (internal flow)	$Nu_{d_t}^{B} = 0.023 Re_{d_t}^{4/5} Pr^{0.3}$

Table 4: Specification of process design parameters considered for evaluating the process and economics performance of the biocrude production plant based on the design shown in Figures 1-4.

Process Parameter	Value
Total input power, $\dot{H}_S^F$	150-600 MW
Woody biomass to organic waste weight mass ratio, $\dot{M}_{wood}^F / \dot{M}_{waste}^F$	50-100%
Moisture in woody biomass (max), $y_{lw,H2O}^F$	40-60%
Moisture in organic waste (max), $y_{lw,H2O}^F$	60-80%
Dryer pressure, P_g^D	1.01 bar-g

Steam temperature to dryer, $T_{g,i}^{D}$	150-200 ºC
Gas to total volume ratio in dryer, ϕ_g^D	0.9
Torrefaction temperature, T_g^T	225 – 275 ºC
Torrefaction pressure, P_r^T	1.01 bar-g
Torrefaction residence time, t_R^T	30-60 min.
Gas to total volume ratio in torrefaction, ϕ_g^T	0.82
Feedstock moisture after pretreatment, $y_{j,H2O}^{PR}$	< 10%
Solid particle size after pretreatment, $d_{j,p}^{PR}$	< 1 mm
Fuel input power in EFG, $\dot{H}_{in}^{G}$	150-600 MW
EFG Pressure, P_g^G	25 bar-g
EFG Temperature, T_g^G	1300-1600 ºC
Gasification lambda value, λ_g	0.2-0.4
ASU outlet O_2 concentration, $x_{O_2}^{ASU}$	95%
Inlet syngas temperature to WGS, $T_{g,0}^{WGS}$	160 ºC
Maximum Temperature WGS, T_r^{WGS}	600 ºC
Max. temperature difference in heat exchangers	10 ºC
Syngas CO_2 concentration after CO2 capture, x_{CO2}^{CCS}	5 % vol.
Inlet syngas temperature to CO2 capture absorber, $T_{g,i}^{ABS}$	15-35 ºC
Inlet Selexol temperature to CO2 capture absorber, $T_{sel,i}^{ABS}$	30 ºC
Selexol absorber pressure, P_g^{ABS}	10 bar-g
Temperature Selexol flash tank, T_{sel}^{FL}	100 ºC
CO_2 supply pressure, P_{CO2}^{CCS}	100 Bar-g
CO_2 supply temperature, T_{CO2}^{CCS}	30 ºC
FT Reactor Temperature, T_r^{FT}	250 ºC
FT Reactor Pressure, P_r^{FT}	25 bar-g
FT CO conversion factor γ_r^{FT}	40-80%
Pressure at separation of biocrude products, P_{bc}^{S}	25 bar-g
Temperature at separation of LNG, T_{LNG}^{S}	-195 ºC

Pressure at separation of LNG, P_{LNG}^{S}	1.01 bar-a
Inlet feed water temperature, T_{fw}	15 ºC
Outlet process water, T_{pw}	25 ºC
Steam Pressure, P_{stm}	25 bar-g
Steam Temperature (superheated), T_{stm}	250 ºC
Steam Intermediate Pressure (IP), P_{stm}^{IP}	25 bar-g
Steam Low Pressure (LP), P_{stm}^{LP}	10 bar-g

Table 5: Main mass flow rates for the biocrude production plant, as shown in Figure 1, calculated for a reference plant capacity of 150 MW as a function of the main input parameters of the analysis, i.e., the mass fraction of the sludge in the raw feedstock Y^F_{sludge}, the gasification lambda value λ_g and the gasification temperature T^G_g. The moisture content of the logwood and the sludge are assumed to be 50 and 60% wt. respectively, with torrefaction temperature and residence time equal to 30 minutes and 225 °C.

Y^F_{sludge} w/w	λ_g -	T^G_g °C	$\dot{M}^F_S$ kg/h	$\dot{M}^G_S$ kg/h	$\dot{M}^G_g$ kg/h	$\dot{M}^{WGS}_g$ kg/h	$\dot{M}^{CC}_{CO2}$ kg/h	$\dot{M}^{CC}_g$ kg/h	$\dot{M}_{bc}$ kg/h	$\dot{M}_{LNG}$ kg/h
0	0.20	1300	51318	27994	40908	54210	6328	40877	15221	1789
0	0.25	1300	51318	27994	47710	53143	6017	36212	12504	1470
0	0.30	1300	51318	27994	54310	54182	5975	33201	11130	1308
0	0.35	1300	51318	27994	60810	60717	6550	33533	10800	1269
0	0.40	1300	51318	27994	67204	67164	7115	33614	10329	1214
0	0.20	1600	51318	27994	35648	53773	6271	42483	13651	1605
0	0.25	1600	51318	27994	41328	54830	6205	39923	12677	1490
0	0.30	1600	51318	27994	46924	53769	5919	35903	11121	1307
0	0.35	1600	51318	27994	52456	51891	5576	31773	9511	1118
0	0.40	1600	51318	27994	57959	57386	6038	32287	9274	1090
0.25	0.2	1300	57595	30763	48613	48617	5562	30043	11050	1299
0.25	0.25	1300	57595	30763	54805	54778	6111	30436	10788	1268
0.25	0.3	1300	57595	30763	60906	60892	6653	30588	10381	1220
0.25	0.35	1300	57595	30763	66927	67799	7280	31066	9992	1174
0.25	0.4	1300	57595	30763	72926	73858	7817	31117	9425	1108
0.25	0.2	1600	57595	30763	41334	48983	5594	33028	11269	1325
0.25	0.25	1600	57595	30763	46563	47199	5249	29087	9614	1130
0.25	0.3	1600	57595	30763	51753	51463	5592	29066	9247	1087
0.25	0.35	1600	57595	30763	56906	56595	6026	29408	8953	1052
0.25	0.4	1600	56394	30763	62044	61743	6460	29635	8591	1010
0.5	0.2	1300	64425	33678	52706	52713	6016	29041	10977	1290
0.5	0.25	1300	64425	33678	58128	58126	6498	29193	10626	1249
0.5	0.3	1300	64425	33678	63483	64399	7074	29751	10309	1212
0.5	0.35	1300	64425	33678	68821	69789	7552	29838	9814	1154
0.5	0.4	1300	64425	33678	73575	74594	7963	29765	9311	1094
0.5	0.2	1600	64425	33678	44438	45573	5187	27917	9874	1161

0.5	0.25	1600	64425	33678	49021	48899	5442	27634	9452	1111
0.5	0.3	1600	64425	33678	53579	53405	5827	27938	9203	1082
0.5	0.35	1600	64425	33678	58138	57945	6213	28154	8900	1046
0.5	0.4	1600	64425	33678	62665	62475	6596	28301	8552	1005

Table 6: Main energy flows for the biocrude production plant, shown in Figure 1, calculated as a function of the main input parameters of the analysis, i.e., the mass fraction of the sludge in the raw feedstock Y^F_{sludge}, the gasification lambda value λ_g and the gasification temperature T^G_g. The moisture content of the logwood and the sludge are assumed to be 50 and 60% wt. respectively, with torrefaction temperature and residence time equal to 30 minutes and 225 °C.

Y^F_{sludge} w/w	λ_g -	T^G_g °C	$\dot{H}^F_S$ MW	$\dot{H}^G_S$ MW	$\dot{H}^G_g$ MW	$\dot{H}^G_{g,th}$ MW	$\dot{H}^{CC}_g$ MW	$\dot{H}^{FTS}_{bc}$ MW	$\dot{H}^{FTS}_{LNG}$ MW
0	0.20	1300	152	150	132	29	131	117	28
0	0.25	1300	152	150	121	34	115	94	23
0	0.30	1300	152	150	111	38	102	83	20
0	0.35	1300	152	150	102	43	97	80	19
0	0.40	1300	152	150	94	48	92	76	18
0	0.20	1600	152	150	136	30	123	107	26
0	0.25	1600	152	150	124	35	114	98	24
0	0.30	1600	152	150	114	40	99	84	20
0	0.35	1600	152	150	105	45	84	71	17
0	0.40	1600	152	150	96	50	81	69	17
0.25	0.2	1300	146	150	107	34	98	79	19
0.25	0.25	1300	146	150	100	39	95	76	18
0.25	0.3	1300	146	150	92	43	90	73	18
0.25	0.35	1300	146	150	85	47	85	70	17
0.25	0.4	1300	146	150	78	51	78	66	16
0.25	0.2	1600	146	150	108	35	98	81	20
0.25	0.25	1600	146	150	101	40	83	69	17
0.25	0.3	1600	146	150	93	45	79	66	16
0.25	0.35	1600	146	150	86	49	76	63	15
0.25	0.4	1600	146	150	79	54	72	61	15
0.5	0.2	1300	138	150	100	38	96	75	18
0.5	0.25	1300	138	150	94	41	92	72	18

0.5	0.3	1300	138	150	88	45	88	70	17
0.5	0.35	1300	138	150	82	49	82	66	16
0.5	0.4	1300	138	150	76	52	76	63	15
0.5	0.2	1600	138	150	101	39	85	68	16
0.5	0.25	1600	138	150	94	43	81	65	16
0.5	0.3	1600	138	150	88	47	78	63	15
0.5	0.35	1600	138	150	82	51	74	61	15
0.5	0.4	1600	138	150	77	55	70	58	14

Table 7: Main heat flows for the biocrude production plant, shown in Figure 1, calculated as a function of the main input parameters of the analysis, i.e., the mass fraction of the sludge in the raw feedstock Y^F_{sludge}, the gasification lambda value λ_g and the gasification temperature T^G_g. The moisture content of the logwood and the sludge are assumed to be 50 and 60% wt. respectively, with torrefaction temperature and residence time equal to 30 minutes and 225 °C.

Y^F_{sludge} w/w	λ_g -	T^G_g °C	$\dot{Q}^{PR}_g$ MW	$\dot{Q}^{GCC}_{th}$ MW	$\dot{Q}^{GCC}_{pw}$ MW	$\dot{Q}^{FTS}_{th}$ MW	$\dot{Q}^{FTS}_{pw}$ MW	$\dot{Q}_{th}$ MW
0	0.20	1300	13,2	24,6	0,12	31,6	0,45	43,0
0	0.25	1300	13,2	27,4	0,19	25,9	0,37	40,1
0	0.30	1300	13,2	30,6	0,26	23,1	0,33	40,5
0	0.35	1300	13,2	31,5	0,36	22,4	0,32	40,7
0	0.40	1300	13,2	32,4	0,46	21,4	0,30	40,6
0	0.20	1600	13,2	31,8	0,09	28,4	0,40	47,0
0	0.25	1600	13,2	32,6	0,15	26,3	0,37	45,7
0	0.30	1600	13,2	36,0	0,21	23,1	0,33	45,9
0	0.35	1600	13,2	40,9	0,26	19,7	0,28	47,4
0	0.40	1600	13,2	42,8	0,33	19,2	0,27	48,9
0.25	0.2	1300	15,5	26,5	0,22	22,2	0,32	33,2
0.25	0.25	1300	15,5	27,2	0,31	21,7	0,31	33,4
0.25	0.3	1300	15,5	27,9	0,40	21,0	0,30	33,3
0.25	0.35	1300	15,5	28,9	0,50	20,2	0,29	33,5
0.25	0.4	1300	15,5	30,0	0,60	19,1	0,27	33,5
0.25	0.2	1600	15,5	30,7	0,18	22,6	0,32	37,7
0.25	0.25	1600	15,5	35,0	0,22	19,3	0,27	38,7
0.25	0.3	1600	15,5	37,0	0,29	18,6	0,26	40,0

0.25	0.35	1600	15,5	38,7	0,36	18,0	0,26	41,2
0.25	0.4	1600	15,5	40,4	0,44	17,3	0,25	42,2
0.5	0.2	1300	18,5	25,8	0,30	21,9	0,31	29,2
0.5	0.25	1300	18,5	26,4	0,38	21,3	0,30	29,2
0.5	0.3	1300	18,5	27,4	0,47	20,7	0,29	29,5
0.5	0.35	1300	18,5	28,3	0,55	19,7	0,28	29,5
0.5	0.4	1300	18,5	29,1	0,63	18,7	0,27	29,3
0.5	0.2	1600	18,5	33,2	0,21	19,6	0,28	34,2
0.5	0.25	1600	18,5	35,1	0,27	18,8	0,27	35,4
0.5	0.3	1600	18,5	36,5	0,33	18,4	0,26	36,4
0.5	0.35	1600	18,5	38,0	0,40	17,8	0,25	37,3
0.5	0.4	1600	18,5	39,5	0,47	17,1	0,24	38,1

Table 8: Cost associated factors to estimate the total permanent investment [46]

Cost associated factors	Abbreviation	Value
Site preparation	f_{site}	0.05 -0.2
Buildings	$f_{building}$	0.05-0.1
Land	f_{land}	0.05-0.1
Cost of contingency	f_{cont}	0.05-0.15
Engineering	f_{eng}	0.02-0.05
Project development and licenses	f_{dev}	0.02-0.03
Commissioning	f_{com}	0.1

Table 9: Parameters' values to estimate the feedstock supply cost, based on data from Trømborg et al. [48] and assuming a exchange rate of 8 Norwegian Krone (NOK) per dollar.

Biomass supply variables	Value

Logwood density, ρ_{lw}	400 kg/m^3
Logwood availability, $m_{lw,S}$	10 tons/ha
Production cost logwood deliver at road, $c_{lw,pr}$	25-31.25 \$/ m^3
Cost of chipping and storage, c_{chip}	6.05 \$/ m^3
Production cost sludge, $c_{sl,pr}$	-50 - 0 NOK/ m^3
Transportation cost (fixed), $c_{tr,f}$	3 \$/ m^3
Transportation cost (variable), $c_{tr,L}$	0.075 \$/ m^3/km

Table 10: Unit cost associated to direct operating cost

Direct Operational Cost	Unit cost
Slag disposal	40 \$ /ton
WGS catalyst	3.63 \$/kg
Physical solvent (Selexol)	5 \$/kg
FT catalyst	13636 \$/m^3
Process water disposal	8.34 \$/m^3
Fresh water	0.4865 \$/m^3

Table 11: Indirect operational cost and reference values

Indirect (Fixed) Operational Cost	value
Average labor hourly rate, c_r	67.9 \$/hour
Operating labor burden	0.3
Overhead factor (operators only)	20%
Labor overhead charge rate	1.25
Administration	2% C_{TPI}

Insurance	1% C_{TPI}
Income tax rate	30 %

Table 12: Unit operating costs, per unit output bioenergy energy, for the base 150 MW plant

Logwood to sludge ratio	100 %	75 %	50 %
Feedstock supply (sludge at 0 $/ton)	11.23	10.05	8.32
Feedstock supply (sludge at 10 $/ton)	11.23	8.51	4.99
Feedstock supply (sludge at 50 $/ton)	11.23	2.36	-8.33
Catalysts	0.69	0.62	0.79
Chemicals	3.69	3.28	4.22
Wastes disposal (solid, effluents)	0.48	0.65	1.24
Labor cost	7.97	7.09	9.11
Maintenance	6.42	5.84	7.72
Utilities	2.48	2.21	2.96
Administration	2.06	2.05	1.96
Insurance	1.03	1.02	0.98

Table 13: Financial assumptions considered for evaluating the cost of biocrude production

Financial parameter	Values/assumptions
Debt equity ratio	70-30
Depreciation model	Straight line depreciation model, depreciation period 20 years
Construction and commissioning duration	3 year period
% required capital during construction and commissioning	30% year 1, 50% year 2 and 20% year 3
Return of Investment	10%

Loan repayment period	10 years
Interest rate	7 %
Currency	US $
Plant cost update	CEPCI 2016
Heat price	78 $/ MWh
LNG price	24 $/MWh
CO_2 credits	50-70 $/ton

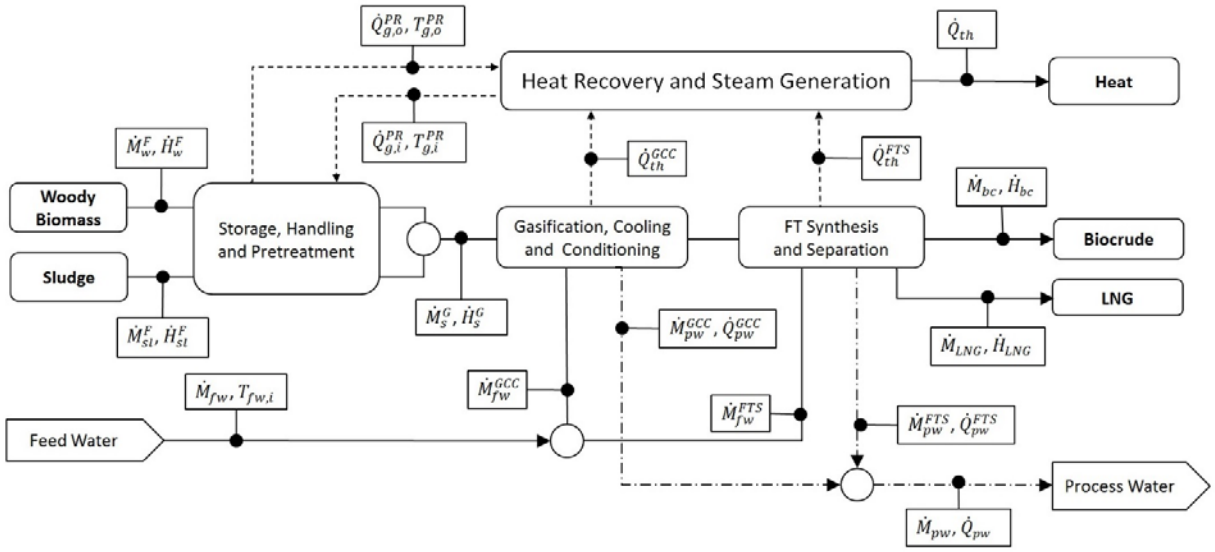

Figure 1: Overall process block diagram for the Fischer-Tropsch biocrude production plant based on co-processing woody biomass and wet organic waste, including the main mass and energy flows.

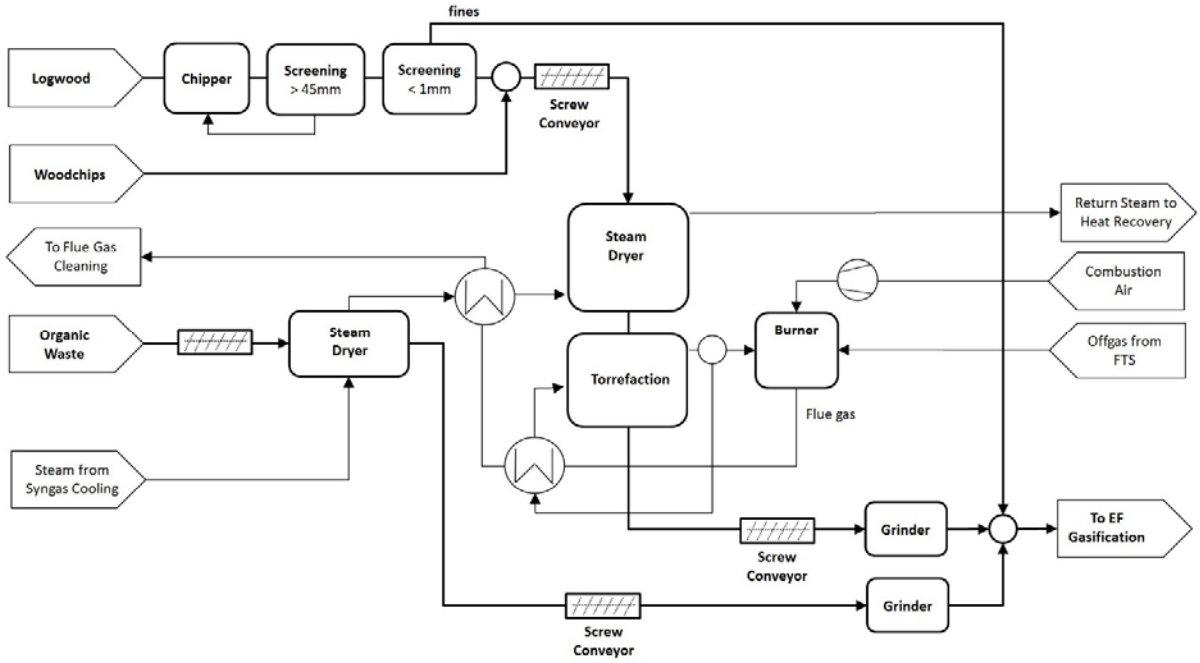

Figure 2: Process flow diagram for the integrated pretreatment of the woody biomass and the organic waste

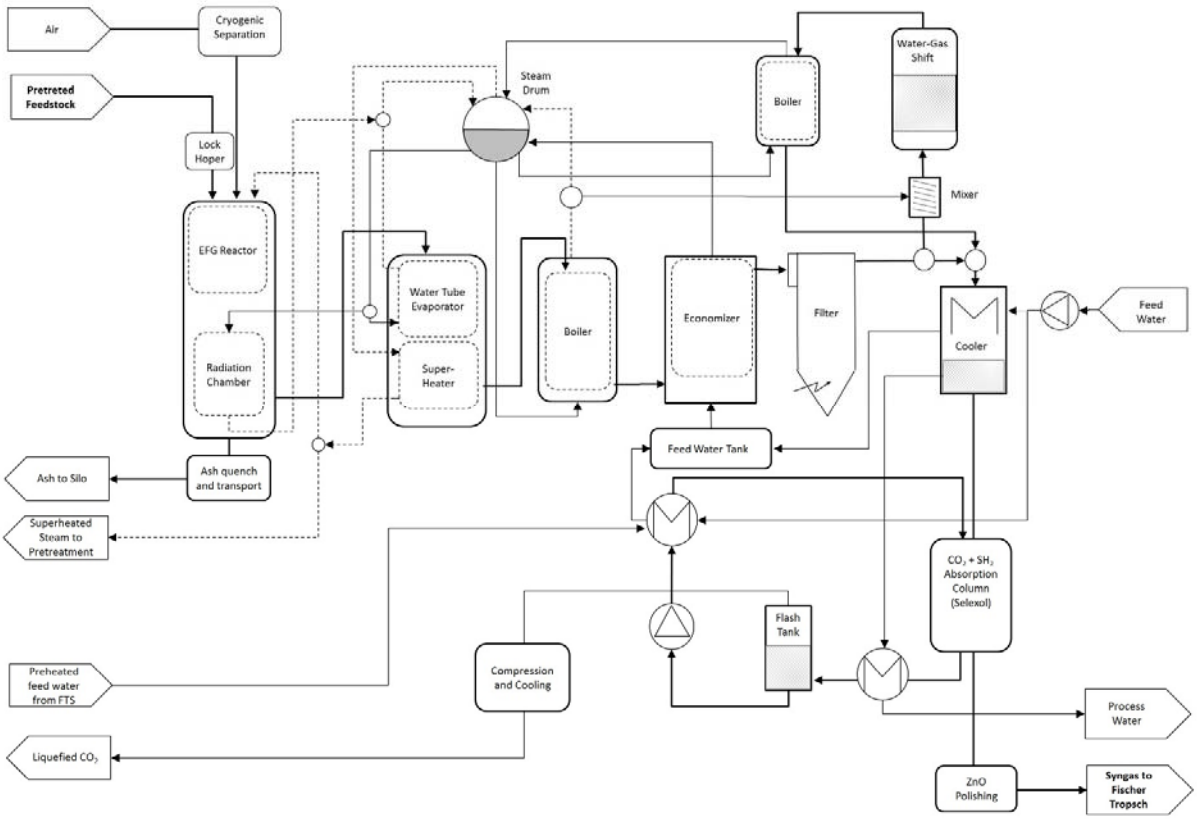

Figure 3: Process flow diagram for the EFG and the syngas cooling and conditioning systems with integration of the heat recovery and steam generation

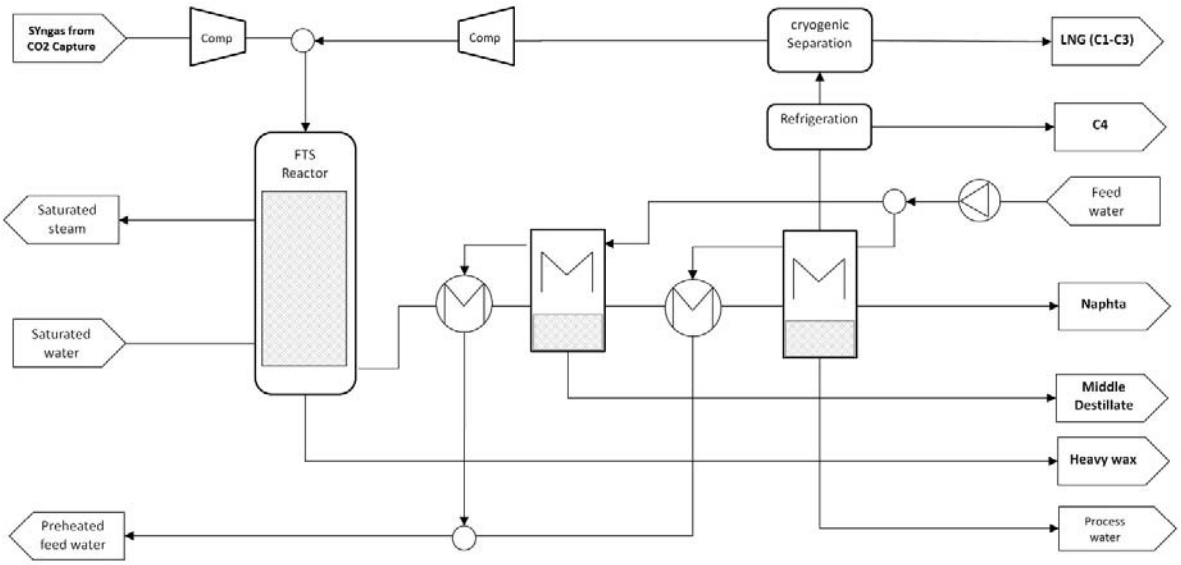

Figure 4: Process Flow Diagram of the FTS system and products separation

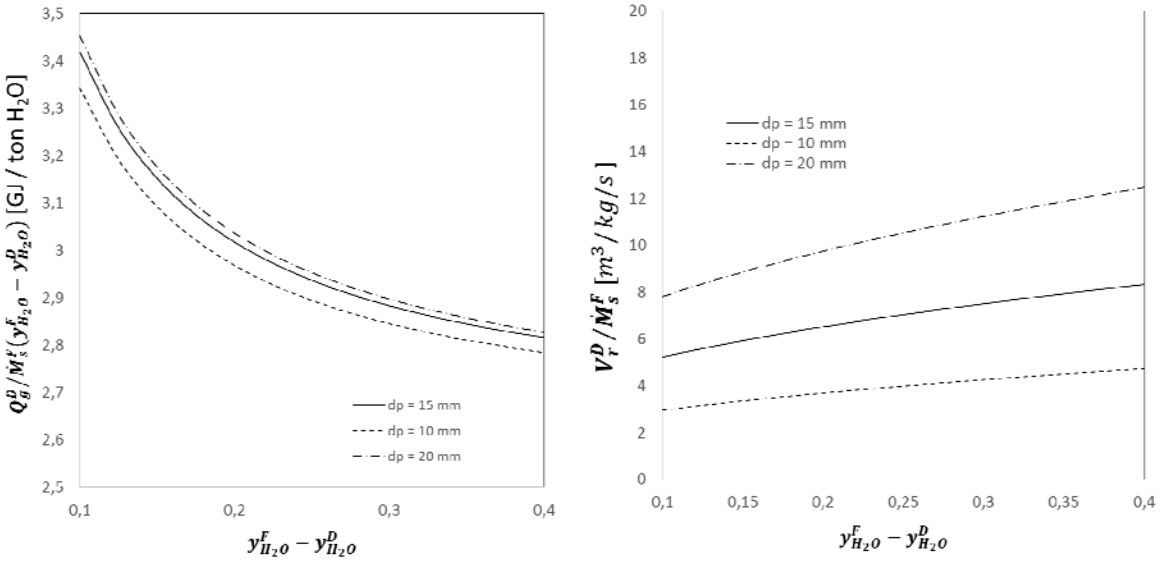

Figure 5: Variation of (a) the thermal power of steam used for drying per unit mass of evaporated water and (b) the dryer volume per unit mass flow rate of feedstock as a function of the moisture content reduction in the dryer for feedstock particle size of 10, 15, 20 mm.

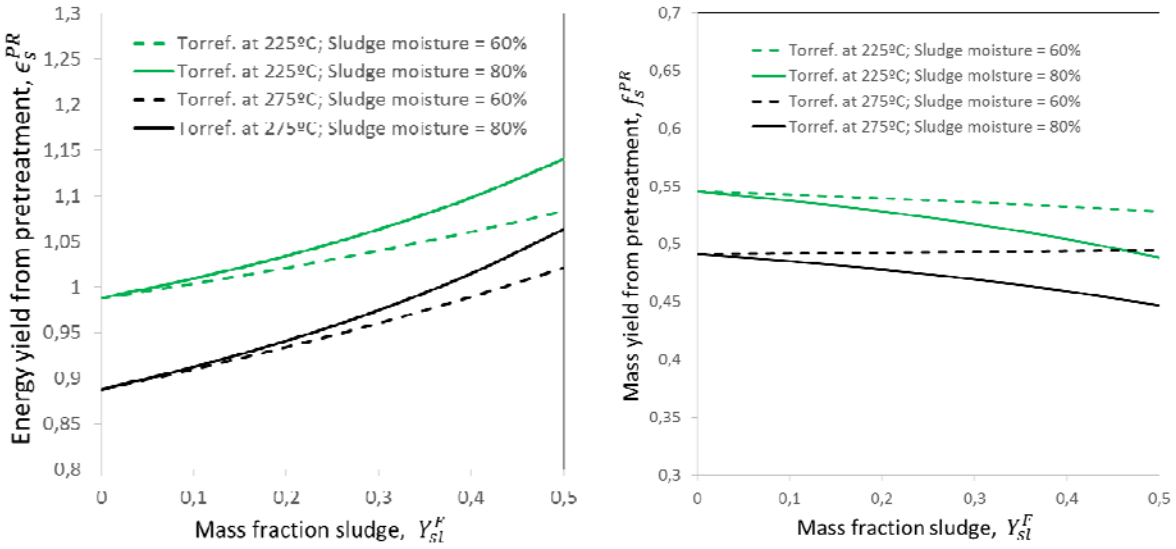

Figure 6: Variation of the energy and mass yields for the overall pretreatment process as a function of the mass fraction of sludge in the input raw feedstock, for torrefaction temperature of 225 and 275 °C, moisture content in the wood of 40% and moisture content in the sludge of 60 and 80 %wt.

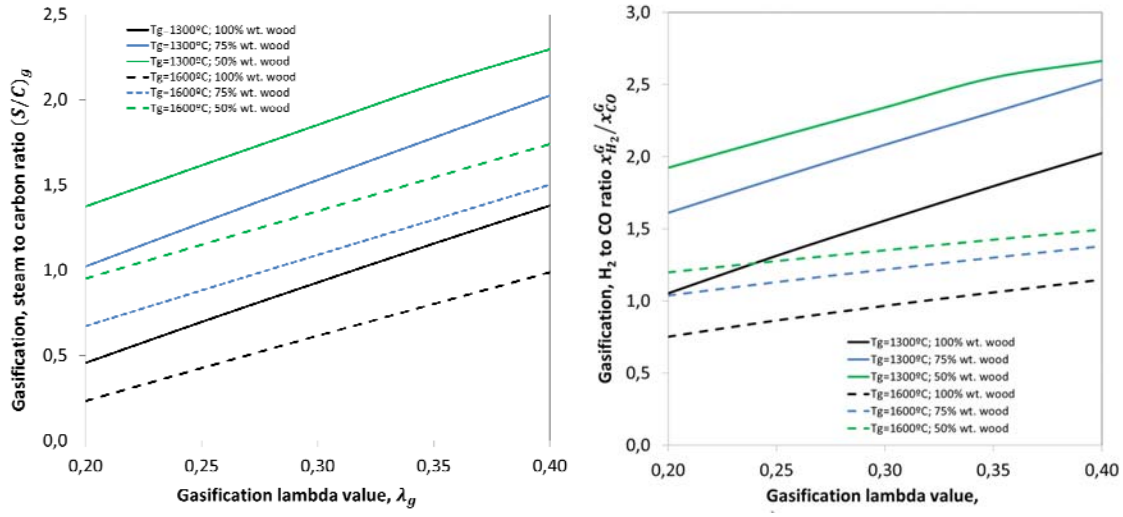

Figure 7: a) Operational limits of the EFG process for variable values of the mass fraction of wood relative to the total input raw feedstock; b) Variation of the H_2 to CO molar ratio of the syngas leaving the EF gasification for the operational limits

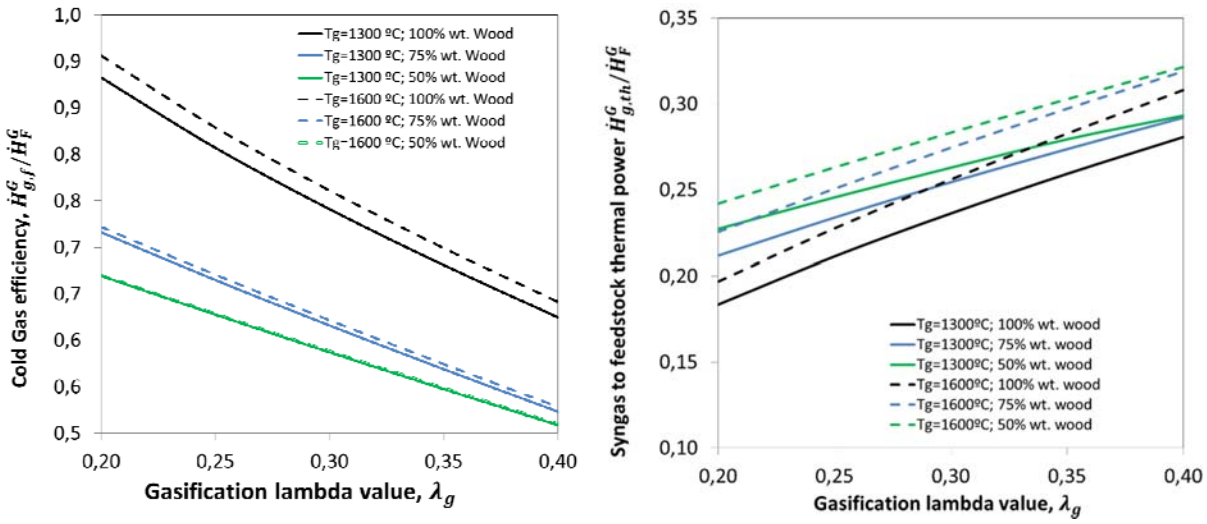

Figure 8: Variation of the (a) cold-gas efficiency and (b) the output thermal energy per unit feedstock energy in the EFG process as a function of the lambda value for variable values of the mass fraction of wood relative to the total input raw feedstock, evaluated from equations (3.3) and (3.4)

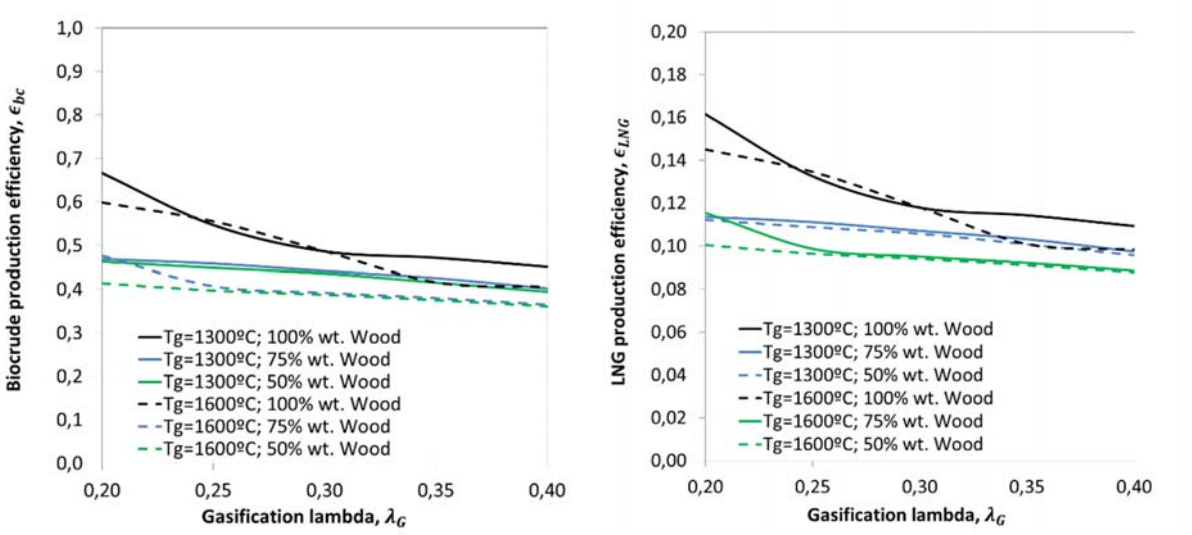

Figure 9: Variation of the biocrude (a) and LNG (b) production efficiency as a function of the gasification lambda value and the raw feedstock composition, evaluated from equations (3.5) and (3.6)

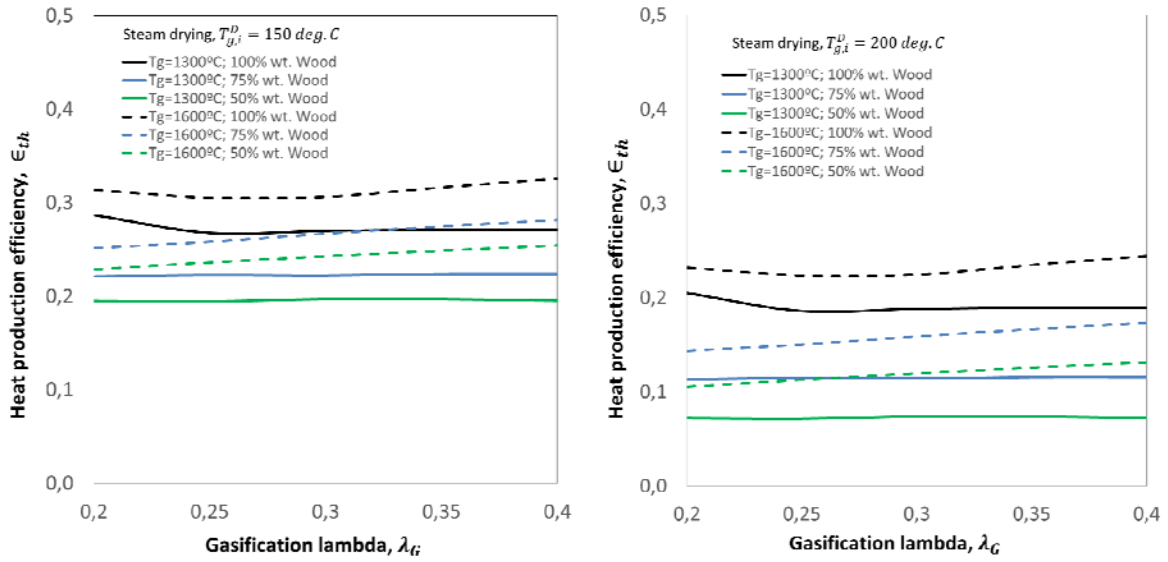

Figure 10: Variation of the net thermal power production relative to the input biomass power to the gasification unit as a function of the operating conditions in the EFG reactor and the raw

feedstock composition, for steam temperature in the dryers equal to 150 ºC (a) and 200 ºC (b). The moisture content in the wood and the sludge is assumed to be, respectively, 50 and 60 % wt.

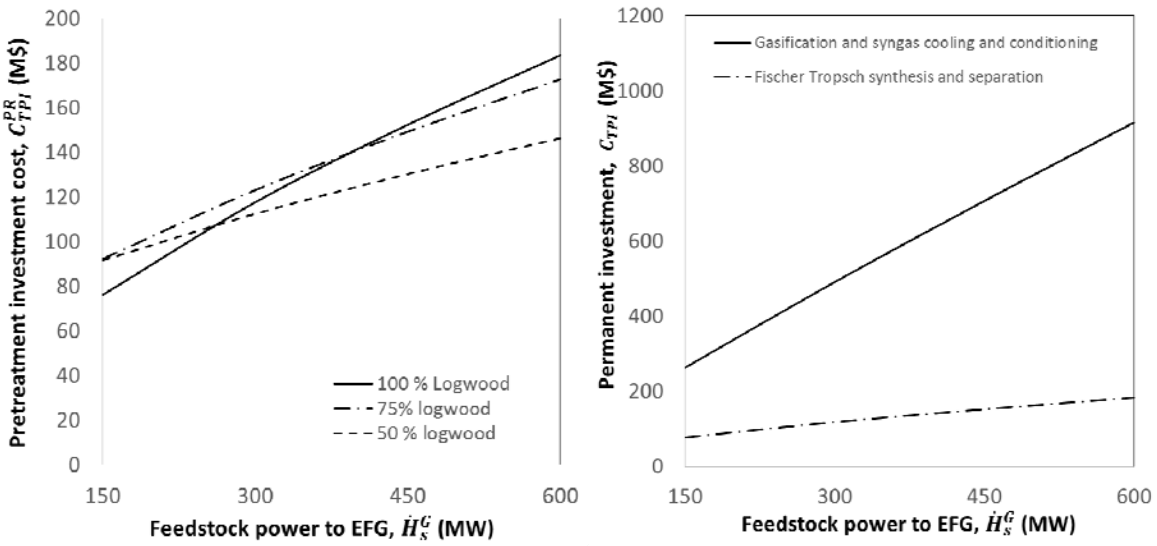

Figure 11: Variation of the total permanent investment as a function of the input feedstock power to the EFG of the pretreatment system, for values of the mass fraction of wood in the input raw feedstock of 0, 25 and 50%, and for the gasification and syngas cooling and conditioning and the Fischer Tropsch and separation systems. The moisture content of the wood and the sludge are assumed to be, respectively, 50% and 80%.

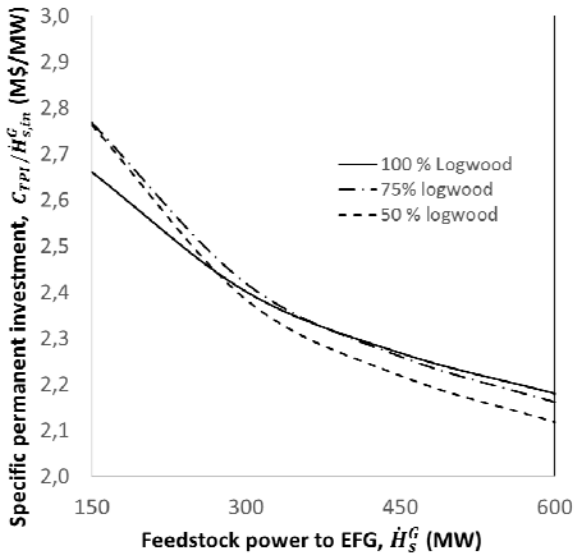

Figure 12: Variation of the specific capital cost of the biocrude production plant as a function of the input feedstock power to the EFG and for values of the mas fraction of wood in the input raw feedstock of 0, 25 and 50%. The moisture content of the wood and the sludge are assumed to be, respectively, 50% and 80%.

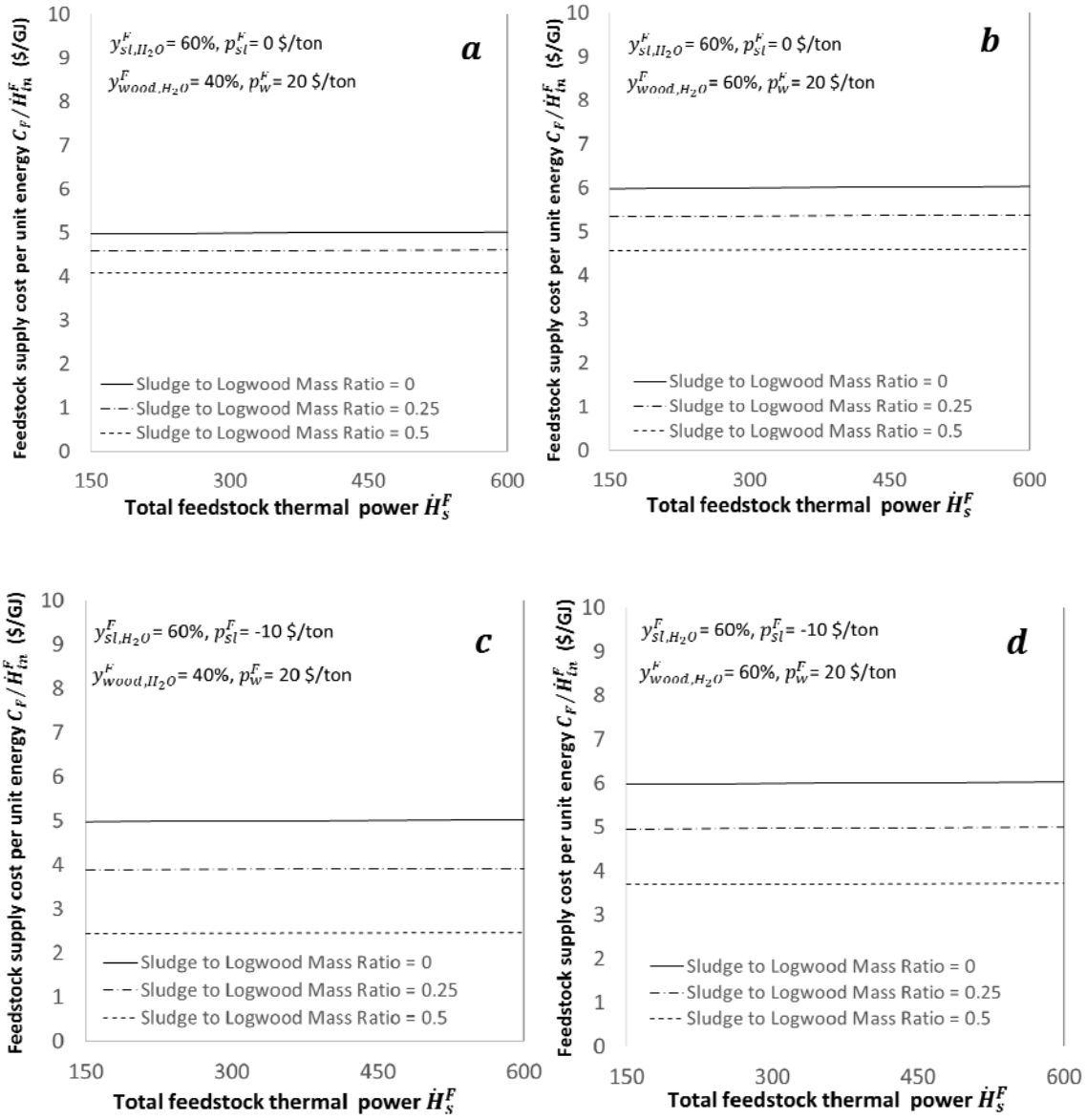

Figure 13: Variation of total cost of feedstock supply per unit input feedstock energy flow to the plant as a function of the plant capacity for values of the mas fraction of wood in the input raw feedstock of 0, 25 and 50%, assuming a moisture content in the sludge of 60 % wt. and a constant price of logwood at road of 20$/ton, a sludge production cost of 0 and -10 $/ton and moisture content in the logwood of 40 and 60 % wt.

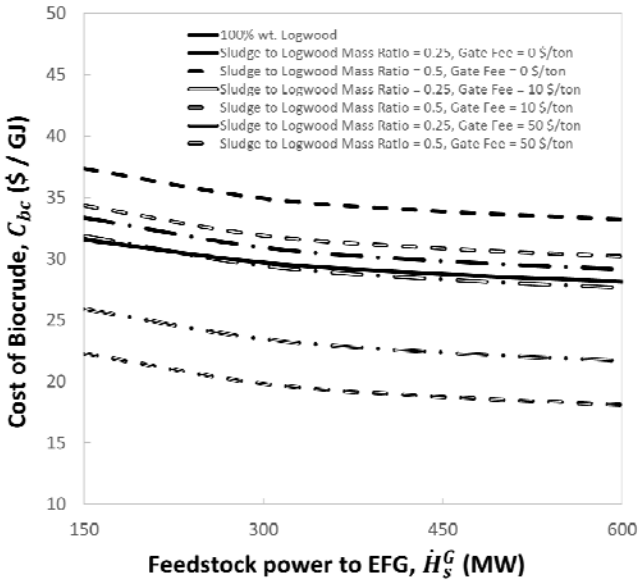

Figure 14: Variation of the cost of biocrude produced from co-processing logwood and sludge from anaerobic digestion as a function of the plant scale, for values of the mass fraction of sludge in the total raw feedstock of 0, 25 and 50% and for gate fees for the sludge at source of 0, 10 and 50 $/ton. It is assumed that the moisture content of the logwood and the sludge are constant and equal to 50 and 60% wt., respectively, and that the price of logwood delivered at road is also constant and equal to 20 $/ton.